
USF Tampa Graduate Theses and Dissertations

USF Graduate Theses and Dissertations

2007

A 1400-year multi-proxy record of climate variability from the northern Gulf of Mexico

Julie N. Richey
University of South Florida

Follow this and additional works at: <https://digitalcommons.usf.edu/etd>

 Part of the American Studies Commons

Scholar Commons Citation

Richey, Julie N., "A 1400-year multi-proxy record of climate variability from the northern Gulf of Mexico" (2007). *USF Tampa Graduate Theses and Dissertations*.
<https://digitalcommons.usf.edu/etd/2338>

This Thesis is brought to you for free and open access by the USF Graduate Theses and Dissertations at Digital Commons @ University of South Florida. It has been accepted for inclusion in USF Tampa Graduate Theses and Dissertations by an authorized administrator of Digital Commons @ University of South Florida. For more information, please contact digitalcommons@usf.edu.

A 1400-Year Multi-Proxy Record Of Climate Variability From The Northern Gulf Of
Mexico

by

Julie N. Richey

A thesis submitted in partial fulfillment
of the requirements for the degree of
Master of Science
College of Marine Science
University of South Florida

Major Professor: Benjamin P. Flower, Ph.D.
David J. Hollander, Ph. D.
Terrance M. Quinn, Ph.D.
Richard Z. Poore, Ph.D.

Date of Approval:
April 10, 2007

Keywords: little ice age, medieval warm period, foraminifera, climate change, holocene

© Copyright 2007 , Julie Richey

TABLE OF CONTENTS

LIST OF TABLES	ii
LIST OF FIGURES.....	iii
ABSTRACT	iv
CHAPTER ONE	1
INTRODUCTION	1
Geographic Setting.....	2
METHODS	3
Mg/Ca Analysis	5
SST Equations	6
PIGMY BASIN SST RECORD	7
Implications for Late Holocene Climate Extremes.....	8
OXYGEN ISOTOPE AND FAUNAL RECORDS	10
Links to High-Latitude Circulation.....	11
CONCLUSIONS	13
CHAPTER TWO	15
INTRODUCTION	15
Background.....	16
METHODS	17
RESULTS AND DISSCUSSION	18
Carbon isotopes.....	18
Oxygen Isotopes.....	20
Mg/Ca.....	22
No size relationship in white <i>G. ruber</i> ?	23
CONCLUSIONS	23
REFERENCES	42
APPENDICES	46
Appendix I: Data table for white <i>G. ruber</i>	47
Appendix II: Data table for pink <i>G. ruber</i>	51
Appendix III: Faunal data (% abundance)	55
Appendix IV: Sea-surface salinity estimates	59

LIST OF TABLES

Table 1	Core-top Mg/Ca.....	25
Table 2	Theoretical calculations of $\delta^{18}\text{O}_{\text{seawater}}$ and SST	25

LIST OF FIGURES

Figure 1	Map of the Gulf of Mexico.....	26
Figure 2	Age model for core PBBC-1	27
Figure 3	Time series of [Al], [Fe] and [Mn] in core PBBC-1	28
Figure 4	Scatter plot of [Al], [Fe] and [Mn] versus Mg/Ca	29
Figure 5	Comparison of calculated SST using different calibration equations.....	30
Figure 6	Mg/Ca-derived SST Record and Northern Hemisphere reconstruction ...	31
Figure 7	Overplot of raw Mg/Ca record from white and pink <i>G. ruber</i>	32
Figure 8	Pigmy Basin % <i>G. sacculifer</i> , $\delta^{18}\text{O}_{\text{calcite}}$ and GISP2 ssNa.....	33
Figure 9	Calculated $\delta^{18}\text{O}_{\text{seawater}}$	34
Figure 10	Comparison of $\delta^{18}\text{O}_{\text{seawater}}$ with % abundance <i>G. ruber</i> (white).....	35
Figure 11	Model of Gulf of Mexico salinity during the month of April	36
Figure 12	Size fraction versus $\delta^{13}\text{C}$ for white and pink <i>G. ruber</i>	37
Figure 13	<i>G. ruber</i> $\delta^{13}\text{C}$ record (pink and white)	38
Figure 14	Size Fraction versus $\delta^{18}\text{O}$ for white and pink <i>G. ruber</i>	39
Figure 15	Size fraction versus Mg/Ca for <i>G. ruber</i> (pink)	40
Figure 16	Size fraction versus Mg/Ca for <i>G. ruber</i> (white).....	41

A 1400-Year Multi-Proxy Record of Climate Variability From the Northern Gulf of Mexico

Julie N. Richey

ABSTRACT

A continuous, decadal-scale resolution multi-proxy record of climate variability over the past 1400 years in the northern Gulf of Mexico (GOM) was constructed from a box core recovered in the Pigmy Basin. Proxies include paired analyses of Mg/Ca and $\delta^{18}\text{O}$ in the white variety of the planktic foraminifer *Globigerinoides ruber* and relative abundance variations of *G. sacculifer* in the foraminifer assemblages. Two multi-decadal intervals of sustained high Mg/Ca values indicate GOM sea-surface temperatures (SSTs) were as warm or warmer than near-modern conditions between 1000 and 1400 yrs BP. Foraminiferal Mg/Ca values during the coolest interval of the Little Ice Age (ca. 250 yrs BP) indicate that SST was 2 - 2.5 °C below modern SST. Four minima in the Mg/Ca record between 900 and 250 yrs BP correspond with the Maunder, Spörer, Wolf and Oort sunspot minima, suggesting a link between solar insolation and SST variability in the GOM. An abrupt shift recorded in both $\delta^{18}\text{O}_{\text{calcite}}$ and relative abundance of *G. sacculifer* occurs ~600 yrs BP. The shift in the Pigmy Basin record corresponds with a shift in the sea-salt-sodium (ssNa) record from the GISP2 ice core, linking changes in high-latitude atmospheric circulation with the subtropical Atlantic Ocean.

CHAPTER 1

INTRODUCTION

Establishing the geographic pattern and magnitude of natural climate variability in the late Holocene is important for anticipating and understanding the likely patterns of future climate change. A number of detailed climate records spanning the last 1 to 2 thousand years (ky) demonstrate that climate of the late Holocene contains high-amplitude variability. Regional patterns and individual records during recent cold and warm extreme climate states, known respectively as the Little Ice Age (LIA) and the Medieval Warm Period (MWP) are complex and highly variable. Cooling/warming in one region may be associated with warming/cooling or no change in another region and individual proxy records may represent local climate phenomena, and are not necessarily representative of hemispheric patterns (e.g., see summary in Crowley and Lowery, 2000).

Hemispheric temperature reconstructions (e.g., Mann and Jones, 2003) that are based on a large number of temperature-sensitive proxy records with variable spatial and temporal resolution result in a record in which variability over the past 1000 years, prior to 1900_{AD}, is subdued (≤ 0.5 °C). The resulting low-amplitude reconstruction contrasts with several individual marine records that indicate centennial-scale SST oscillations of 2-3 °C occurred during the last 1000-2000 years (i.e., Keigwin, 1996; Lund and Curry, 2005; Watanabe et al., 2001, Newton et al., 2006). Tree-ring and multi-proxy reconstructions designed to capture multi-centennial-scale variability (e.g. Esper et al.,

2002; Moberg et al., 2005), also suggest that the amplitude of natural climate variability over the past 1000 years is larger than 0.5 °C. Thus there is conflicting evidence on the amplitude of late Holocene decadal to century-scale climate variability. Resolving these discrepancies requires the continued development of quality high-resolution late Holocene climate records.

Geographic Setting and Regional Climatology

Here we present a continuous, decadal-scale-resolution marine record from the Pigmy Basin (Fig.1), located on the continental slope in the northern Gulf of Mexico (GOM) (27°11.61 N, 91 °24.54 W, water depth 2259 m). The intraslope basins of the Texas-Louisiana Slope in the north central GOM are formed by the faulting associated with active salt diapirism. The Pigmy Basin is defined as a blocked-canyon intraslope basin, formed by an upward moving salt diapir blocking a former submarine canyon (Bouma and Coleman, 1986). Deposition in the Pigmy Basin is primarily hemipelagic, and thus its high sedimentation rate (43 cm/ky) allows for high-resolution studies in the late Holocene. The influx of continental material via the Mississippi River makes it an ideal setting for recording not only sea-surface variability but also hydrologic changes over the North American continent.

During the boreal summer (July, August, September) the Western Hemisphere Warm Pool (WHWP) extends into the GOM, with sea-surface temperature (SST) exceeding 28.5 °C throughout. The WHWP, which extends from the eastern North Pacific Ocean through the GOM and Caribbean and into the tropical Atlantic, is the dominant heat source for the Western Hemisphere extratropics during the summer, and is

the primary moisture source driving the North American Monsoon (Wang and Enfield, 2002). The GOM is closely linked to the Caribbean and tropical Atlantic via the Loop Current, which is a surface-ocean current that brings warm waters from the Caribbean Sea through the Yucatan Strait into the GOM before exiting through the Florida Straits to be incorporated into the Gulf Stream.

The GOM is a significant source of moisture to the North American continent, and thus studies of hydrologic variability during the late Holocene are relevant to predicting future changes in North American precipitation. The GOM region has one of the highest rates of evaporation minus precipitation (E-P) in the North Atlantic basin. The mean annual E-P rate is 150-175 cm/yr, and rates are highest in the winter and spring when they reach 225-250 cm/yr (Schmitt et al., 1989). The net evaporation in the GOM-Caribbean region can be attributed to the trade winds, which originate in the region of subtropical high and progress toward the equator. Higher sea-level pressure (SLP) in the subtropical Atlantic leads to higher trade wind intensity, which is positively correlated with increased net evaporation in the western subtropical Atlantic (Giannini et al., 2000). This suggests a strong link between atmospheric circulation and hydrologic variability in the GOM.

METHODS

Age control for Pigmy Basin box core PBBC-1 is based on 7 AMS ^{14}C dates (Fig.2). Raw radiocarbon dates were converted to calendar years using the CALIB 5.0 Program with a 400-year reservoir correction (Stuiver et al., 1998). Calibrated ages were plotted against core depth, and a least squares regression ($R^2=0.995$) indicates a linear

sedimentation rate of 43 cm/ky (within the errors of the calibrated dates) and a core-top age of 0 yrs BP. Thus we infer that the data from the youngest samples in our record represent near-modern conditions, or an average of the last 30-50 years. The age model with a sampling interval of 0.5 cm results in an average sample resolution of 12 years throughout the record.

Sediment samples were processed for faunal, isotopic and elemental analyses using standard procedures (Poore et al., 2004). The relative abundance of *Globigerinoides sacculifer* in the planktic foraminifer assemblage for each sample was determined from faunal census counts of ~300 specimens in the >150 μ m size fraction. Oxygen isotope and elemental analysis was performed on 40-80 pooled *Globigerinoides ruber* (white variety) from the 250-300 μ m size fraction of each sample. The restricted 250-200 μ m size fraction was used for geochemical analyses because studies have indicated that there is a relationship between foraminiferal test size and isotopic and elemental ratios. Oxygen isotope ratios were measured on a ThermoFinnigan Delta Plus XL light stable isotope ratio mass spectrometer (SIRMS) at the College of Marine Science, University of South Florida (CMS, USF). The $\delta^{18}\text{O}_{\text{calcite}}$ is reported on the VPDB scale, based on the NBS-19 standard. Average precision for $\delta^{18}\text{O}_{\text{calcite}}$ is $\pm 0.09\text{ ‰}$, based on replication of 15 % of the samples (n=20 replicates). Elemental analyses were performed on a Perkin Elmer Optima 4300 dual view inductively coupled plasma optical emission spectrometer (ICP-OES) at the CMS, USF. Average precision for Mg/Ca values is $\pm 0.16\text{ mmol/mol}$, based on 40% duplicate and triplicate samples (n=45 replicated samples). This corresponds to $\pm 0.4\text{ }^{\circ}\text{C}$.

Mg/Ca Analysis

In preparation for elemental analysis, samples underwent a rigorous cleaning process according to the procedure of Barker et al. (2003). The major steps include the mechanical removal of clay minerals, oxidation of organic matter and acid leaching to remove adsorbed metals. Fe and Al concentrations are measured simultaneously with Mg and Ca, and can be used as indicators of the presence of silicate contamination. Clay minerals make up a significant portion of GOM sediments, and these minerals are composed of 1-10% Mg by weight (Barker et al., 2003). Therefore ineffective removal of clay minerals during the cleaning process could result in artificially high Mg/Ca. In Figure 3, [Al], [Fe] and [Mn] are plotted in a time series with Mg/Ca to verify that Mg/Ca does not covary with silicate contaminants. To further illustrate this point, Al, Fe and Mn concentrations are plotted against Mg/Ca in a scatter diagram (Fig. 4). R^2 values are <0.2 indicating that there is no significant relationship between silicate contaminants and Mg/Ca.

An additional reductive step outlined in the Cd/Ca cleaning procedure from Boyle and Keigwin (1985), is used in some studies (i.e. Lund and Curry, 2006) to remove Mn-Fe-oxides from diagenetic overgrowth, but was determined to be unnecessary for Mg/Ca analysis by Barker et al. (2003). Pena et al. (2005) found that Mg/Ca is reduced by 7-36% after the reductive cleaning step, but have not shown conclusively that this is due exclusively to removal of high-Mg material within the diagenetic overgrowth phases. Figure 3 illustrates that the occurrence of elevated Mn concentrations does not coincide with high Mg/Ca. Samples from the top 10 cm of core PBBC-1 have Mn concentrations close to zero, suggesting that diagenetic processes have not occurred in the youngest part

of the core. A reductive cleaning step may artificially lower the Mg/Ca of the core-top samples relative to those down-core samples that contain Mn-oxide overgrowth.

SST Equations

We determined a mean Mg/Ca core-top value of 4.43 mmol/mol (± 0.03) for the Pigmy Basin from analyses of 0-0.5 cm samples from three sub-cores of PBBC-1 (Table 1). Converting Mg/Ca to an SST estimate is not straightforward because there are significant differences between existing calibration equations used to derive SST estimates from Mg/Ca. For example the Pigmy Basin core-top Mg/Ca value of 4.43 mmol/mol results in a temperature estimate of 25.4 °C using the *G. ruber* equation of Anand et al. (2003), and 27.2 °C using the equation of Dekens et al., (2002). However, both equations yield temperature records with identical amplitudes because they use the same exponential constant of 0.09. Figure 5 shows a comparison of the SST record using the Anand et al., (2003) and Dekens et al., (2002) calibration equations, and illustrates the effect of changing the exponential and pre-exponential constant in the equation. We chose to calculate SST using the *G. ruber*-specific equation with a fixed exponential constant from Anand et al., (2003) [$[\text{Mg/Ca}=0.449*\exp(0.09*\text{SST})]$], because it yields a core-top SST value of 25.4 °C, equivalent to the modern annual average for the GOM (Levitus, 2003). Due to the lack of a calibration equation specific to the GOM-Caribbean region, as well as the discrepancy in absolute SST values between calibration equations, we focus on comparison of the PBBC-1 record to Pigmy Basin core top Mg/Ca, and highlight the amplitude of temperature change but not the absolute SST estimates.

PIGMY BASIN SST RECORD

Seasonal flux data from the Sargasso Sea indicate that the white variety of *G. ruber* is abundant in surface waters throughout the year (Deuser et al., 1987), therefore we follow previous work (Flower et al., 2004, LoDico et al., 2006) and interpret variation in Mg/Ca of *G. ruber* (white variety) as a proxy for mean annual SST. The main features of the Mg/Ca record from PBBC-1 (Fig. 6a) include two multi-decadal intervals of sustained high Mg/Ca (> 4.4 mmol/mol) between 1000 and 1400 yrs BP that are separated by a multi-decadal interval of lower Mg/Ca. A >0.4 mmol/mol shift to lower mean Mg/Ca occurred at about 1000 yrs BP, and lower but variable mean Mg/Ca (mean=3.8 mmol/mol) occurred between 900 and 300 yrs BP. After 250 yrs BP, mean Mg/Ca increased by 0.4 mmol/mol towards the core-top value of 4.4 mmol/mol. In Figure 7, the Mg/Ca of the pink variety of *G. ruber* is plotted with the white *G. ruber* Mg/Ca curve to illustrate that the same pattern and amplitude of variability is observed in a different variety of *G. ruber*.

The total amplitude of variability in mean Mg/Ca (~ 1.4 mmol/mol) indicates a temperature range of ~ 3 $^{\circ}$ C from the maxima between 1000 and 1400 yrs BP to the SST minima occurring between 900 and 300 yrs BP. The sustained multi-decadal-long intervals of high Mg/Ca between 1000 and 1400 yrs BP are at the beginning of the time range associated with the MWP (ca. 800 to 1200 yrs BP; Broecker, 2001). The mean Mg/Ca in the Pigmy basin record from 1000-1400 yrs BP exceeds the core-top value by ~ 0.4 mmol/mol, while 11 individual measurements exceed the core-top value by >0.6 mmol/mol. Thus our data provide evidence for mean annual SST in the northern Gulf of Mexico as warm or warmer than near-modern SST during the early part of the MWP.

Minima in Mg/Ca, defined by intervals lasting >50 years in which the Mg/Ca is more than 0.6 mmol/mol lower than the core-top value (> 1.5°C cooler), are present at ~ 850 yrs BP, 700 yrs BP, 450 yrs BP and 250 yrs BP. The youngest three minima fall within the age range associated with the LIA (Crowley and Lowery, 2000). Six individual Mg/Ca measurements between 850 and 250 yrs BP are more than 1 mmol/mol lower than the core-top value, indicating that SST in the northern GOM was as much as 2.0 to 2.5 °C cooler than near modern SST during several intervals of the LIA. The four Mg/Ca minima coincide with the Oort, Wolf, Spörer and Maunder Minima in the sunspot record, respectively. Thus it is likely that the variability in the Pigmy Basin SST record is linked to centennial-scale variability in solar insolation.

Implications for late Holocene climate extremes

The magnitude of cooling indicated by Pigmy Basin Mg/Ca during cold extremes of the LIA near 250 and 450 yr BP is ~2.0–2.5 °C which coincides generally with the cold intervals of the LIA centered at 1800_{AD} and 1600_{AD} (Crowley and Lowery, 2000). Oxygen isotopic and Mg/Ca temperature estimates from coral records from Puerto Rico indicate a LIA cooling of 1.5 °C ca.1800_{AD} and 2 °C ca.1700 _{AD} (Winter et al., 2000; Watanabe et al., 2001). Sr/Ca temperature estimates from Bermuda coral ca.1850_{AD} indicate a cooling of at least 1.0 °C (Goodkin et al., 2005). SST estimates based on $\delta^{18}\text{O}$ in the planktonic foraminifer *G. ruber* (white) from the Sargasso Sea suggest a cooling of ~1–2 °C 300–400 yr BP (Keigwin, 1996). Thus the ~2.0–2.5 °C LIA cooling derived from the Pigmy Basin is consistent with published LIA cooling estimates from the Caribbean and subtropical western Atlantic.

Lund and Curry (2006) obtained 4 Mg/Ca SST records from the Dry Tortugas and the Great Bahama Bank in the subtropical western Atlantic that each show very different patterns of variability over the past \sim 1400 yr. However, all 4 records indicate SST during parts of the LIA was on the order of 1.0 $^{\circ}$ C cooler than modern. In addition, Great Bahama Bank core 125 MC indicates SST ca.1200–1300 yr BP was similar to modern SST. Newton et al. (2006) developed sub-decadal resolution Mg/Ca SST record from the western tropical Pacific that exhibits an amplitude of SST variability over the past 1500 years that is similar to that of the Pigmy Basin SST record. Temperature maxima ca. 1000 yr BP are similar to modern SST and temperature minima during the LIA were 1.0 $^{\circ}$ C to 1.5 $^{\circ}$ C below modern. Thus, the near modern or slightly warmer than modern Pigmy Basin SST estimates ca. 1000 yr BP are supported in part by published estimates from the subtropical western Atlantic.

The Pigmy Basin Mg/Ca record is compared in Figure 6 to a Regional Curve Standardization (RCS) climate reconstruction derived from tree-ring records at 14 sites in the Northern Hemisphere (Esper et al., 2002). The RCS record is developed from mid to high-latitude (30–70 $^{\circ}$ N) and high-elevation sites in the Northern Hemisphere. We chose to compare our record to the Esper et al. (2002) reconstruction because they utilized statistical techniques that preserve multi-centennial climate variability after the data are processed. The Pigmy Basin Mg/Ca record and the RCS climate reconstruction show similar patterns of variability. For example, both indicate maximum cooling ca.200 and 400 yr BP. Both records contain a multi-decadal warm interval ca.1000 yr BP indicating temperature as warm or warmer than near modern temperature. Results of Blackman-Tukey cross-spectral analysis between the 2 records indicate a significant coherence (at

the 95% significance level) at periods >200 yr. The similarity of the Pigmy Basin Mg/Ca and RCS records indicates a linkage between extratropical continental temperature variability and northern Gulf of Mexico SST on multi-centennial timescales. Small differences in the timing of climate extremes between the two records fall within the errors of the independent age models.

OXYGEN ISOTOPIC AND FAUNAL RECORDS

The relative abundance of *Globigerinoides sacculifer* in the planktic foraminifer assemblages and the $\delta^{18}\text{O}$ of *G. ruber* from core PBBC 1 are plotted with the sea-salt-sodium (ssNa) record from the GISP2 Ice core in Figure 8. *Globigerinoides sacculifer* (Fig. 8a) is abundant in the Caribbean and variations in the *G. sacculifer* abundance in the northern GOM sediments are related to the influx of Caribbean surface waters into the GOM and the average position of the ITCZ (Poore et al., 2004). The most prominent feature in the *G. sacculifer* record is an abrupt shift to lower relative abundance at 600 yrs BP.

Interpretation of the $\delta^{18}\text{O}$ record is complicated because the $\delta^{18}\text{O}$ is influenced by changes in SST and the isotopic composition of seawater. The major feature of the mean $\delta^{18}\text{O}$ *G. ruber* record (Fig 8b) is a rapid shift to more positive values at about 600 yrs BP. Prior to 600 yrs BP the mean record is fairly stable with the exception of a decadal-scale excursion to more positive values ca. 1050_{AD}. After the shift at 600 yrs BP, the $\delta^{18}\text{O}$ record contains several well-defined oscillations that culminate in a trend to more negative values over the last 100 years.

Paired Mg/Ca and $\delta^{18}\text{O}$ measurements can be used to calculate seawater $\delta^{18}\text{O}$ ($\delta^{18}\text{O}_{\text{seawater}}$). The $\delta^{18}\text{O}_{\text{seawater}}$ may then be interpreted in terms of salinity variations (see Appendix IV for discussion of salinity calculations). Given the unresolved uncertainties in the absolute Mg/Ca-SST estimates that are used as an input into the equation for deriving $\delta^{18}\text{O}_{\text{seawater}}$, we present the PBBC-1 $\delta^{18}\text{O}_{\text{seawater}}$ curve (Fig. 9) here to illustrate major trends in $\delta^{18}\text{O}_{\text{seawater}}$ variability, but do not attach significance to minor fluctuations or absolute numerical $\delta^{18}\text{O}_{\text{seawater}}$. The major features of the $\delta^{18}\text{O}_{\text{seawater}}$ curve include two maxima centered near 500 and 1050 yrs BP. The older excursion coincides with the sustained interval of high SST centered at 1050 yrs BP (see Fig. 6), as well as a multi-decadal excursion of higher $\delta^{18}\text{O}_{\text{calcite}}$ (see Fig. 8). The younger excursion coincides with the mean shift observed in both the *G. sacculifer* and $\delta^{18}\text{O}_{\text{calcite}}$ records (see Fig. 8). The $\delta^{18}\text{O}_{\text{seawater}}$ record also covaries inversely with the % abundance of *G. ruber* (white) in core PBBC-1, with the two maxima in $\delta^{18}\text{O}_{\text{seawater}}$ corresponding to minima in the % abundance of the white variety of *G. ruber* (Figure 10). This inverse relationship between $\delta^{18}\text{O}_{\text{seawater}}$ and % abundance of *G. ruber* (white) was also observed in a mid-Holocene GOM record from the Orca Basin (Lodico et al., 2006).

Links to high-latitude circulation

Analysis of a glaciochemical series of major ions in an ice core from Greenland (GISP2) has revealed a distinct shift in ssNa concentrations at 600 yr BP (Meeker and Mayewski, 2002). When the most recent 100 years of the ssNa series is compared to the instrumental record of sea-level pressure (SLP) in the North Atlantic, a strong positive relationship between ssNa concentration and intensity of the Icelandic Low (IL) is

revealed (Meeker and Mayewski, 2002). A more pronounced (deeper) IL results in increased winter winds blowing from the North Atlantic onto Greenland increasing the ssNa content of the ice. Thus the long-term ssNa record (Fig 8c) is considered a proxy for variability in the IL.

The ssNa record contains an abrupt shift in mean values at 600 yrs BP that is synchronous within dating errors with the abrupt shifts to lower values in the *G. sacculifer* and $\delta^{18}\text{O}$ record from PBBC-1. The shift in ssNa is interpreted as an atmospheric circulation change resulting in a deeper IL and more intense winter circulation over the North Atlantic at the beginning of the Little Ice Age (Meeker and Mayewski, 2002). Cross-spectral analysis (using the Blackman-Tukey method) between the Pigmy Basin $\delta^{18}\text{O}$ record and the GISP2 ssNa record indicate significant coherence (at the 95% confidence level) at periods >200 years. The close correspondence at centennial timescales coupled with the synchronous mean shift observed in both records ca. 600 yrs BP indicates a link between atmospheric circulation in the North Atlantic and the subtropical Atlantic.

The decrease in *G. sacculifer* abundance at 600 yrs BP suggests a southward shift in the average position of the ITCZ and a reduced influx of Caribbean surface water coincided with the intensification of the IL. The concurrent shift to more positive $\delta^{18}\text{O}_{\text{seawater}}$ is also consistent with a southward migration of the average position of the ITCZ, which would result in reduced summer transport of moisture into the GOM region. No change in Mg/Ca is associated with the shift in the $\delta^{18}\text{O}$ and *G. sacculifer* records, indicating that the change in regional hydrology ca. 600 yrs BP is not linked with a major change in GOM SST.

Over the instrumental period, positive ssNa anomalies are highly correlated with an increased SLP gradient between the IL and the Bermuda High (BH) (Meeker and Mayewski, 2002). The intensification of winter trade winds associated with a larger IL-BH gradient could increase evaporation in the trade-wind belt, thus producing the positive $\delta^{18}\text{O}_{\text{seawater}}$ excursions in the Pigmy Basin record that coincide with increases in ssNa in the GISP2 record ca. 600 yrs BP and 1050 yrs BP. These positive $\delta^{18}\text{O}_{\text{seawater}}$ excursions are not likely the result of decreases in freshwater input from the Mississippi River. Figure 11 shows modeled sea surface salinity for the GOM in April, the month of maximum Mississippi discharge. During maximum freshwater input, the lower-salinity plume is confined to the coastal areas, moving eastward and westward along the shelf, and thus has little influence on the surface salinity over the Pigmy Basin. Therefore, it is likely that the hydrologic variability over the past 1400 years in the Pigmy Basin region is being driven by changes in net evaporation, and not Mississippi input.

CONCLUSIONS

Close correspondence of the Pigmy Basin Mg/Ca record to the NH climate reconstruction of Esper et al. (2002) demonstrates coherence between high latitude terrestrial climate and subtropical Atlantic SST. Raw Mg/Ca during two multi-decadal intervals between 1000 and 1400 yrs BP suggest SST was as warm or warmer than near-modern SST at that time. Pigmy Basin Mg/Ca data also suggest SST cooling during intervals of the LIA that was at least 2 $^{\circ}\text{C}$ below near-modern SST. The overall amplitude of SST variability in the Pigmy Basin record during the past 1400 years is about 3 $^{\circ}\text{C}$,

75% of the glacial-interglacial SST difference estimated in the GOM (Flower et al., 2004).

SST and hydrologic changes are de-coupled on multi-decadal to centennial timescales in the GOM. The abrupt shift in $\delta^{18}\text{O}_{\text{calcite}}$ and *G. sacculifer* abundance from the Pigmy Basin ca. 600 yrs BP coincides with a rapid change in atmospheric circulation as inferred from the GISP2 ssNa record from Meeker and Mayewski (2002). The data suggest a strong linkage between atmospheric circulation changes in the high latitude North Atlantic and the hydrologic changes in subtropical Atlantic at \sim 600 yrs BP, but not with SST.

CHAPTER 2

INTRODUCTION

The incorporation of minor elements and stable isotopes into biogenic carbonates is governed by a number of physiological and environmental parameters, both equilibrium and non-equilibrium. When utilizing elemental and isotopic ratios in foraminiferal calcite for the purpose of paleoceanographic reconstructions, the goal is to maximize the environmental signal and to minimize non-equilibrium fractionation factors. Contributing factors to non-equilibrium fractionation include metabolic fractionation (Berger et al., 1978), photosynthesis and respiration of symbionts (Spero and Lea, 1993), and kinetic effects (McConaughey, 2003).

As a foraminifer grows its metabolic rate, depth habitat, and symbiont condition change, and thus the offset of test geochemistry from equilibrium may change. In this study I test the hypothesis that foraminiferal test size has an effect upon Mg/Ca, $\delta^{13}\text{C}$, and $\delta^{18}\text{O}$ values by measuring the isotopic and elemental composition of multiple size classes of the pink and white varieties of the planktonic foraminifer, *Globigerinoides ruber*. Previous studies have shown non-equilibrium fractionation of carbon and oxygen isotopes, as well as Mg/Ca to be related to foraminiferal test size (Berger et al., 1978; Curry and Matthews, 1981; Elderfield et al., 2002; Ravelo and Fairbanks, 1995; and Williams et al., 1981).

Curry and Matthews (1981) measured $\delta^{13}\text{C}$ and $\delta^{18}\text{O}$ in a series of different size fractions of the white *G. ruber* in core-top samples from the Indian Ocean. They found that the carbon isotopic composition of *G. ruber* increased with increasing size, while there was no significant correlation between the oxygen isotopic composition and test size. Elderfield et al. (2002) conducted a similar study involving both white and pink *G. ruber*, and measured Mg/Ca in addition to carbon and oxygen isotopes. Results suggested an increase in $\delta^{13}\text{C}$ with increasing test size for all species analyzed. The influence of test size on $\delta^{18}\text{O}$ and Mg/Ca, however, was less clear. There was a slight increase in Mg/Ca with size in white *G. ruber*, but no relationship in pink *G. ruber*, and there was no significant relationship between test size and $\delta^{18}\text{O}$ in white or pink *G. ruber*.

The material used in the Elderfield et al., (2002) study is of mid-Holocene age, and the sampling interval is equivalent to 800 years per sample. They used only 20 individual foraminifers per measurement, so it is possible that their different size fractions were biased toward distinct climate regimes within that 800-year period, and thus the variability observed may not reflect the true influence of size on test geochemistry. With the Pigmy Basin material, the core-top material used represents only about 12-years, and thus the possibility of the foraminifera representing different climate extremes is less likely.

BACKGROUND

Oxygen isotopic composition in planktonic foraminifera is the most widely used proxy for making inferences about sea-surface temperature (SST) and salinity (SSS) in the paleoceanographic record. Foraminiferal $\delta^{18}\text{O}$ becomes more depleted with

increasing temperature and decreasing salinity. Carbon isotopes in planktonic foraminifera are more difficult to interpret in terms of a single sea-surface parameter. The carbon isotopic composition of the dissolved inorganic carbon (DIC) pool is fractionated in seawater by a number of environmental processes including biological production, mixing of water masses, and exchange of carbon between different reservoirs. In addition, carbon is fractionated during calcification in biogenic carbonates as the result of endosymbionts, metabolic processes and kinetic effects. In a general sense, carbon isotopes can be interpreted as a productivity proxy. When primary productivity increases, the DIC pool from which the foraminifer calcifies becomes more enriched in $\delta^{13}\text{C}$. Thus, increases in foraminiferal $\delta^{13}\text{C}$ indicate increases in primary productivity.

Foraminiferal Mg/Ca is used as a paleotemperature proxy. This is based on the principle that Mg^{2+} replaces Ca^{2+} in the calcite lattice according to an exponential temperature dependence (i.e. Mg/Ca increases about 9% with a 1°C increase in SST from Anand et al., 2003). During the inorganic precipitation of calcite Mg/Ca increases by 3% per 1°C increase in temperature, indicating a preference for high-Mg calcite in biogenic carbonates. Very little is understood about the mechanisms of elemental fractionation in foraminiferal calcification, or how it might change as a function of test size.

METHODS

For isotopic analysis, 20 individuals of both the pink and white varieties of *G. ruber* were picked from each size fraction from the 10-15mm depth in core PBBC-1. A 5mm sample represents roughly 12 years of time, and the 10-15mm sample was likely deposited in the latter half of the 20th century (see explanation on page 4). Size fractions

analyzed for *G. ruber* (pink) included 150-212 μm , 212-250 μm , 250-300 μm , 300-355 μm and 355-425 μm . Size fractions analyzed for *G. ruber* (white) include the 150-212 μm , 212-250 μm , 250-300 μm and 300-355 μm size fractions. For Mg/Ca, the same size fractions were analyzed, but the experiment was conducted at 2 different depths in core PBBC-1: 20-25mm (~50-100 yrs B.P.) and 320-325mm (~800 yrs B.P.).

RESULTS AND DISCUSSION

Carbon isotopes

Figure 12 shows plots of $\delta^{13}\text{C}$ as a function of size for both pink and white *G. ruber*. There is a positive correlation between size and carbon isotopic composition in both the pink and white *G. ruber* data, with R^2 values of 0.93 and 0.89 respectively. The slopes are nearly identical for both regressions, with the pink variety being enriched by 0.41 per mil relative to the white variety. The average difference between the $\delta^{13}\text{C}$ values of white and pink *G. ruber* was calculated for the 1500-year time series (Figure 13), indicating that pink *G. ruber* is enriched by 0.35 per mil relative to white *G. ruber*, thus illustrating that this isotopic offset is consistent through time. There is a $>1.0\text{ \textperthousand}$ range between the carbon isotopic values of the smallest (150-212 μm) and the largest ($>355\text{ \mu m}$) size fractions of both pink and white *G. ruber*. This range is equivalent to the entire range of variability that is observed in the 1500-year time series of $\delta^{13}\text{C}$ data (Figures 13).

The results generated for $\delta^{13}\text{C}$ versus size are consistent with previous studies (Berger et al., 1978; Curry and Matthews, 1981; Elderfield et al., 2002; Ravelo and Fairbanks, 1995) and the principles of kinetic fraction in symbiont-bearing planktonic

foraminifera. Metabolic processes produce CO₂ that is depleted in ¹³C relative to DIC in seawater. Metabolism is highest during early ontogenetic stages (smaller size fractions), leading to the incorporation of more metabolic CO₂ into foraminiferal calcite. As the foram grows, calcite precipitation continues, but metabolism slows (Berger et al., 1978). Thus, fractionation due to metabolic effects is lowest in the larger size fractions. This trend is clearly illustrated in Figure 12, where there is a positive linear correlation between size and $\delta^{13}\text{C}$.

Photosynthesis of dinoflagellate symbionts also contributes to disequilibrium fractionation of carbon in planktonic foraminifera. During photosynthesis, CO₂ composed of the lighter isotope of carbon is preferentially taken up by the algal symbionts. This carbon is subsequently packaged into low molecular weight metabolites to be utilized during foraminiferal metabolism. This effect is expressed most strongly in the smaller size fractions for multiple reasons. As pointed out in the previous paragraph, metabolism is highest in small individuals. Therefore more photosynthetically fractionated carbon will be incorporated into the tests of juvenile foraminifera. Additionally, foraminifera sink through the water column during their life cycle, leading to decreased photosynthetic activity. There is also fractionation associated with respiration, but Spero and Lea (1986) show that <10% of respired CO₂ is incorporated into the calcite skeleton of the planktonic species, *Orbulina universa*. Most calcification occurs during the day when photosynthesis is more active than respiration (McConaughey, 2003).

In Figure 12, the trend lines for pink and white *G. ruber* have nearly identical slopes, but there is a 0.4‰ offset in the $\delta^{13}\text{C}$ values. A possible cause for the offset in

their $\delta^{13}\text{C}$ values is difference in seasonal distribution of white and pink *G. ruber*. The pink variety of *G. ruber* is confined to the warmest 6 months in the year, with fluxes dropping to zero from December to May (Deuser et al., 1987), while the major phytoplankton blooms occur in the early spring. Increased photosynthesis during the early bloom may leave the carbon pool more enriched in the summer. This phenomenon could account for the $\delta^{13}\text{C}$ values being 0.4‰ higher in pinks than in whites. Whites have a broader seasonal distribution, and thus would not exhibit the elevated $\delta^{13}\text{C}$ values of pinks. There may also be slight differences in the depths of calcification for the two varieties of *G. ruber*. High photosynthetic rates at the surface cause $\delta^{13}\text{C}$ values to be highest at the surface and decrease with depth in the water column. It is possible that pink *G. ruber* is calcifying at a slightly shallower depth in the water column.

Oxygen isotopes

Figure 14 illustrates a significant negative correlation between the oxygen isotopic composition of pink *G. ruber* and test size, with an $R^2=0.92$. The $\delta^{18}\text{O}$ observed in the largest size class of pink *G. ruber* is 0.6 ‰ lower than in the smallest size class. This is equivalent to a 3°C range in temperature space. The $\delta^{18}\text{O}$ data for white *G. ruber*, however, indicate no correlation with size.

Interpretation of data generated for $\delta^{18}\text{O}$ versus size fraction (Figure 14) is not as straightforward as the $\delta^{13}\text{C}$ data. In the pink *G. ruber*, the data indicate a significant negative correlation between size and $\delta^{18}\text{O}$ value. This contradicts the slightly positive relationship between size and $\delta^{18}\text{O}$ in pink *G. ruber* observed by Elderfield et al. (2002). The sampling interval for that study, however, is ~800 years between 4 and 5 ky BP. The

climate variability over that 800-year period is large enough that it may mask the real size- $\delta^{18}\text{O}$ relationship within a sample of 20 individual foraminifera.

The $\delta^{18}\text{O}$ data generated for white *G. ruber* show no relationship to size fraction. This is confounding, since the same carbon fractionation mechanisms seem to be at work in the two varieties of *G. ruber*, based on consideration of the $\delta^{13}\text{C}$ data. The $-0.92\ \delta^{18}\text{O}$ value for the 212-250 μm sample appears to be anomalous, but the value had a high reproducibility. Curry and Matthews (1981) observe a positive relationship between size and $\delta^{18}\text{O}$ in white *G. ruber*, while Elderfield et al., (2002) observe a negative relationship. Curry and Matthews' (1981) core-top samples come from a region in which the annual temperature range is $>25^\circ\text{C}$ (compared to about 9°C in the GOM). The range of calcification temperatures within a small sample size would likely mask any true size- $\delta^{18}\text{O}$ relationship.

Table 2 shows the results of an exercise in which the $\delta^{18}\text{O}$ values generated in this study were used to calculate both $\delta^{18}\text{O}_{\text{seawater}}$ and SST using known modern values as constants in Equation 1. A modern $\delta^{18}\text{O}_{\text{seawater}}$ value of $1.1\text{\textperthousand}$ is used for the GOM (from Fairbanks et al., 1992), and a modern mean summer SST of 28.0°C is used for *G. ruber* (pink) and a modern mean annual SST of 25.4°C is used for *G. ruber* (white) (Levitus, 2003). For *G. ruber* (pink), the $\delta^{18}\text{O}$ data for the 250-300 μm size fraction yields SST and $\delta^{18}\text{O}_{\text{seawater}}$ values that are closest to predicted values. The predicted SST and $\delta^{18}\text{O}_{\text{seawater}}$ values were not produced from any of the size fractions for *G. ruber* (white).

Equation 1: $\text{SST}(\text{ }^\circ\text{C})=14.9-4.8(\delta_c-\delta_{\text{sw}})$ (from Bemis et al., 1998)

Mg/Ca

This size fraction experiment was conducted at two different core depths for both pink and white *G. ruber* to determine whether the size-Mg/Ca relationship was constant through time, and whether it could be replicated. The 20-25 mm represents a modern period (~50-100 yrs B.P.), while the 320-325mm age represents an age of 800 yrs B.P. Figure 15 illustrates a significant positive correlation between test size and Mg/Ca in pink *G. ruber* at two different core-depths. The R^2 values for the 20-25mm and 320-325mm depths are 0.68 and 0.86 respectively. The slopes of the regression lines are identical for the two different depths, with an overall range of 0.8 mmol/mol (2°C) between the smallest and largest size class. The Mg/Ca values are offset because the 320-325mm depth represents a cold period in the Gulf of Mexico relative to the 20th century.

In Figure 16, Mg/Ca is plotted against test size for the white variety of *G. ruber* for the same 2 depth horizons. As observed in the $\delta^{18}\text{O}$ data, there is no significant correlation between size and Mg/Ca. Least squares regression lines are fit through each data set and the R^2 values are < 0.1 . The total range of Mg/Ca variability among the different size fractions is as large as that observed in the 1400-year timeseries from the Pigmy Basin (see Figure 6).

There is clearly a well-defined relationship between size and Mg/Ca values in the pink variety of *G. ruber* (Figure 15). The 0.8 mmol/mol (2°C) range of Mg/Ca values exhibited from the smallest to the largest size class is nearly as large as the LIA to modern range of variability. This illustrates the necessity for determining a limited size range on which to perform elemental analyses.

*No size relationship in white *G. ruber*?*

The lack of an apparent relationship between size and elemental/oxygen isotopic ratios in the white variety of *G. ruber* is perplexing, given the strong relationship exhibited in the pink variety. One hypothesis that could explain the discrepancy invokes the different seasonal distributions of the two varieties. Flux data show two major peaks in the flux of white *G. ruber*: the first occurs in early spring when SSTs are coolest, and the second occurs in late summer when SSTs are warmest (Deuser, 1987). Thus a given sample of white *G. ruber* would record the entire range (9°C) of annual SST variability in the Gulf of Mexico (Levitus, 2003). When using a small sample size of 20 individual foraminiferal tests, it is possible that samples are biased towards a particular season. For instance, a sample of 12 foraminifera may include one individual from each of the 12 months of the year, while another sample includes 10 individuals living in August and 2 from January. Therefore the assumption that both samples represent an annual average is incorrect. Using a larger sample size (i.e. >100 tests) would improve the odds of having a sample representative of annual average conditions. Since it has been established that pinks are living during a more narrow SST range during the year, the data are inherently less noisy.

CONCLUSIONS

While most studies conclude that there is a significant positive relationship between test size and carbon isotopic composition (Berger et al., 1978; Curry and Matthews, 1981; Elderfield et al., 2002; Ravelo and Fairbanks, 1995; Williams et al., 1981), there is little agreement among studies regarding the effect of size on Mg/Ca or oxygen isotopic composition. This study shows a clear effect of test size on elemental

and oxygen isotopic ratios in the pink variety of *G. ruber*, but inconclusive results with respect to white *G. ruber*. An experimental design which could better constrain the environmental conditions under which the foraminifera were calcifying (i.e. culture or sediment trap samples) would help to reveal the source of the discrepancy between the pink and white *G. ruber* data.

The large range of variability observed in $\delta^{13}\text{C}$, $\delta^{18}\text{O}$ and Mg/Ca between the different size fractions of the planktonic foraminifer *G. ruber* illustrates the necessity for choosing a narrow size range on which to perform geochemical analyses. Reducing the effects of non-equilibrium fractionation on test geochemistry will increase the robustness of the environmental variability in the signal.

Core	Sample	Mg/Ca
PBBC-1D	0-5 mm	4.448
PBBC-1A	0-5 mm	4.443
PBBC-1E	0-5 mm	4.398
	Mean	4.429
	Std. Dev.	0.027

Table 1: Core-top Mg/Ca for 3 Pigmy Basin sub-cores. The Mg/Ca of the 250-300 μ m size fraction of *G. ruber* (white) was measured on the core-top samples for each of 3 sub-cores from pigmy Basin box core PBBC-1.

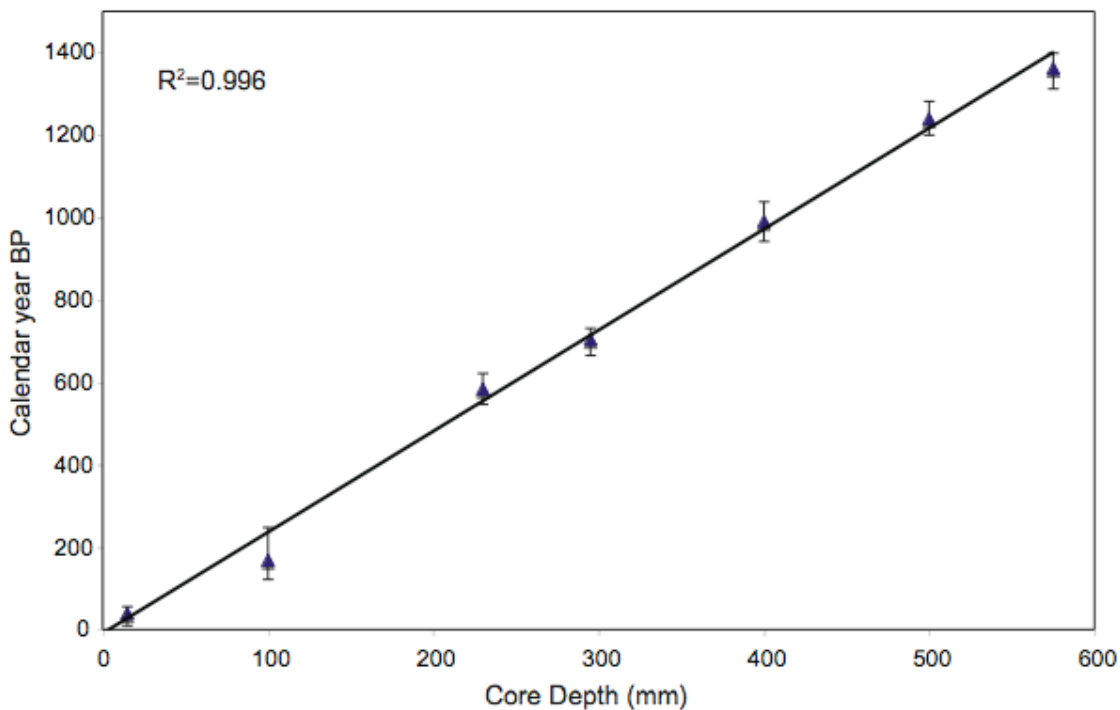
Size (pink)	$\delta^{18}\text{O}$ pink	SST ($\delta\text{w}=1.1$)	δw (SST=28.0°C)
125-150	-1.35	26.93	1.32
212-250	-1.46	27.458	1.21
250-300	-1.58	28.034	1.09
300-355	-1.67	28.466	1.00
>355	-1.94	29.762	0.73

Size (white)	$\delta^{18}\text{O}$ white	SST ($\delta\text{w}=1.2$)	δw (SST=25.4°C)
150-212	-1.33	26.834	0.80
212-250	-0.92	24.866	1.21
250-300	-1.3	26.69	0.83
300-355	-1.19	26.162	0.94

Table 2: Theoretical calculations of $\delta^{18}\text{O}_{\text{seawater}}$ and SST. For each of the size fractions of both pink and white *G. ruber*, SST and $\delta^{18}\text{O}_{\text{seawater}}$ were calculated using measured $\delta^{18}\text{O}_{\text{calcite}}$ and with a modern SST or $\delta^{18}\text{O}_{\text{seawater}}$ values from the literature. The following equation was used for these calculations: $\text{SST}(\text{°C})=14.9-4.8(\delta_{\text{c}}-\delta_{\text{sw}})$ from Bemis et al. (1998). A $\delta^{18}\text{O}_{\text{seawater}}$ value of 1.1‰ was input for pink *G. ruber* and 1.2‰ was input for whites to calculate SST from $\delta^{18}\text{O}_{\text{calcite}}$ (Fairbanks et al., 1992). Modern SST values of 28.0°C and 25.4°C were used as inputs into the equation for pink and white *G. ruber* respectively. These values are the modern summer and annual averages for the GOM (from Levitus, 2003). The highlighted values point out that the $\delta^{18}\text{O}_{\text{calcite}}$ data for the 250-300 μ m size fraction of pink *G. ruber* produce reasonable SST and $\delta^{18}\text{O}_{\text{seawater}}$ values given the assumptions made here.



Figure 1. Map of the Gulf of Mexico. The Pigmy Basin is an intraslope basin in the northern Gulf of Mexico. Core PBBC-1 was raised from a water depth of 2,259 m at (27°11.61 N, 91 °24.54 W).



Depth (mm)	Raw ^{14}C age	Analytical error	Cal Age (yrs BP)	+	-
15-20	350	40 yrs	40	16	31
100-105	535	40 yrs	169	79	48
230-235	1000	40 yrs	584	37	38
295-300	1160	35 yrs	704	27	39
400-405	1445	40 yrs	991	47	49
500-505	1680	40 yrs	1239	43	39
575-580	1825	35 yrs	1362	36	50

Figure 2. Age model for core PBBC-1. The age model is based on 7 AMS ^{14}C dates that were converted to calendar years using the CALIB 5.0 Program with a 400-year reservoir correction (Stuiver et al., 1998). Dates are measured from 8-12 mg samples of mixed planktonic species from the $>150\text{ }\mu\text{m}$ size fraction. (A) A least-squares regression line is fit through the 7 points, giving a linear sedimentation rate with an $R^2=0.995$. (B) Table shows the raw ^{14}C dates with errors and calibrated calendar years with errors.

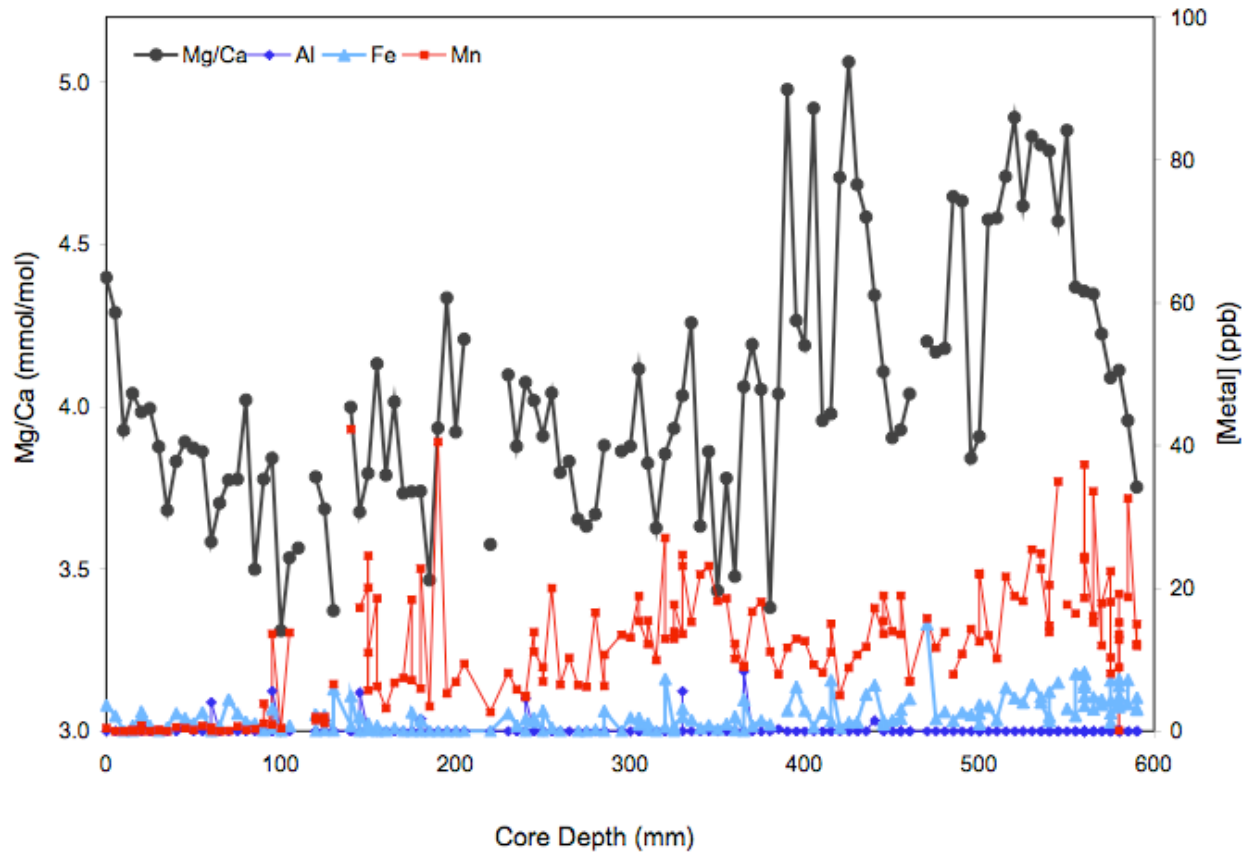


Figure 3. Time series of [Al], [Fe] and [Mn] in core PBBC-1. Mg/Ca (grey) is plotted against core-depth. Corresponding [Fe] (light blue), [Al] (dark blue) and [Mn] (red) are plotted against core-depth to illustrate that silicate and metal-oxide contaminants do not covary with Mg/Ca

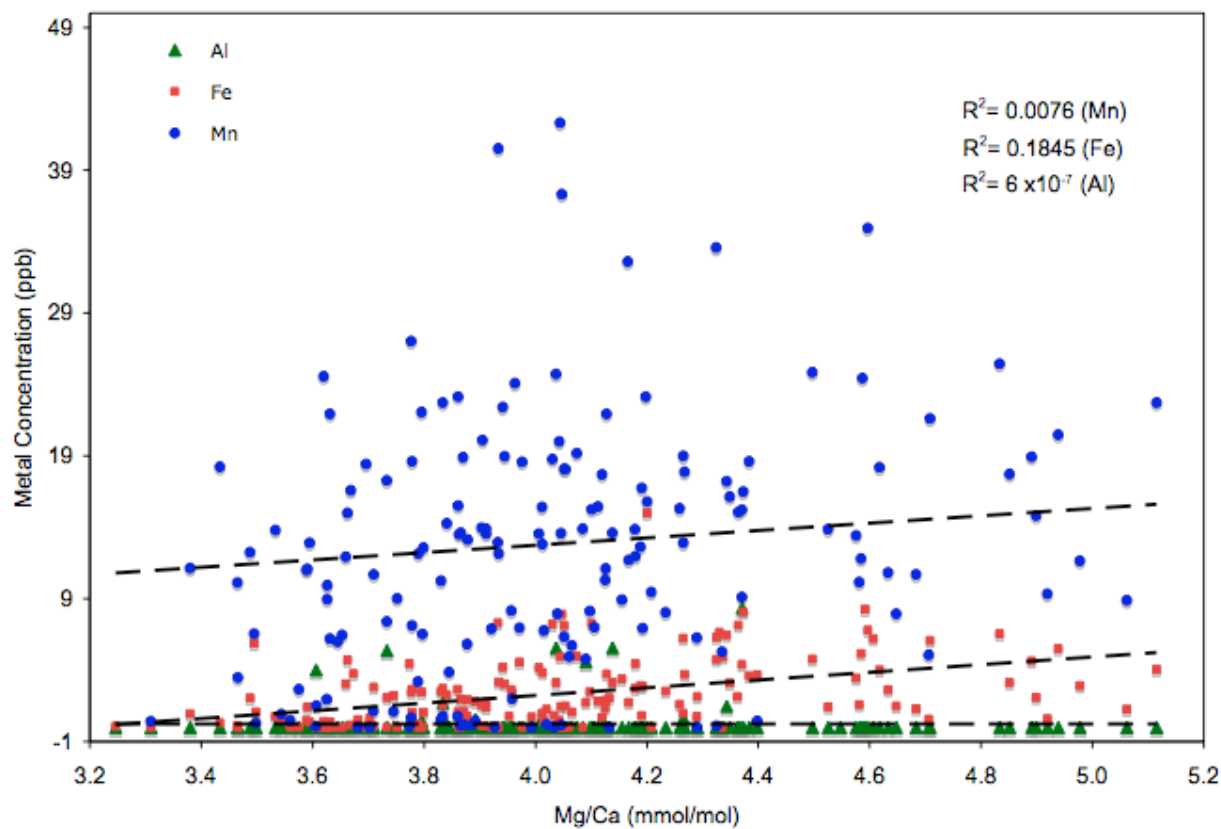


Figure 4. Scatter plot of [Al], [Fe] and [Mn] versus Mg/Ca. Least squares regression lines are fit through each data set, and R^2 values are shown to illustrate that there is no significant relationship between Mg/Ca and Al, Fe or Mn concentrations.

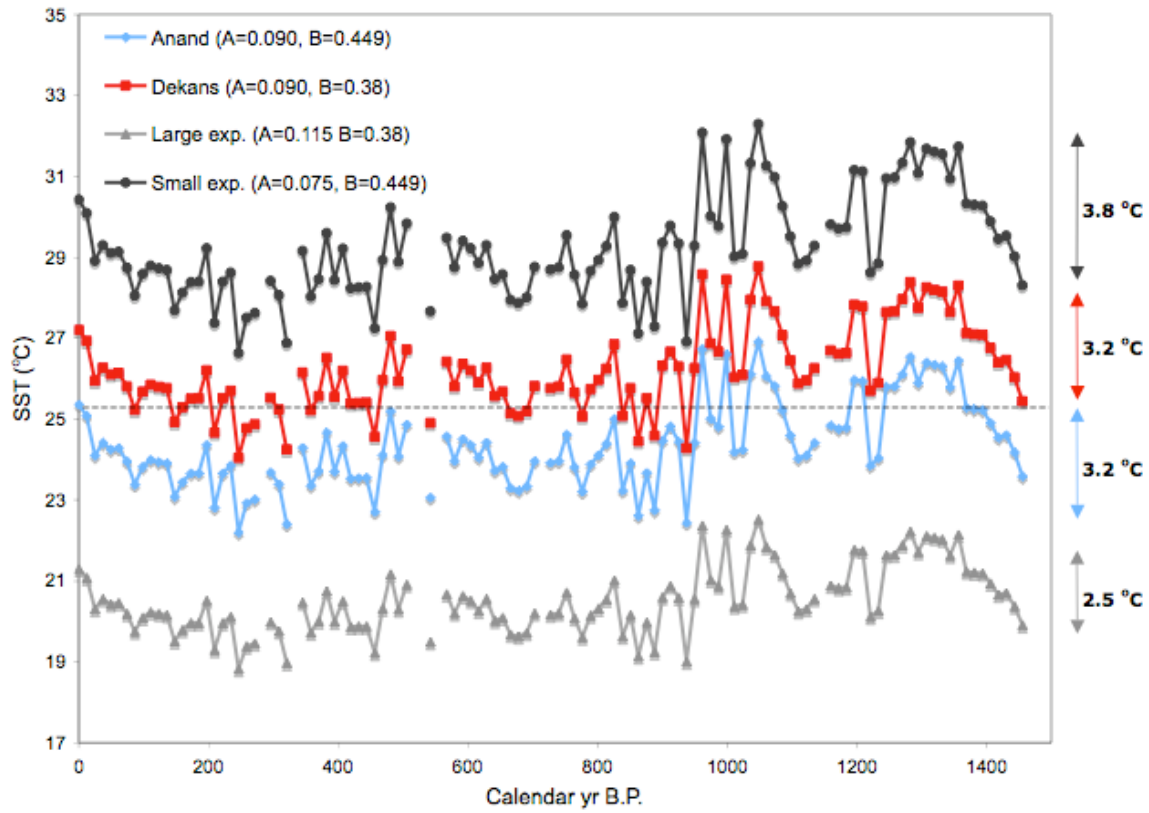


Figure 5. Comparison of calculated SST using different calibration equations. SST is calculated from Mg/Ca according to the exponential equation: $\text{Mg/Ca} = \text{Bexp}(A \cdot \text{SST})$. This figure illustrates the SST record generated using different A and B constants from Anand et al. (2003) (blue), Dekens et al. (2002) (red), an arbitrarily large A (light grey) and an arbitrarily small A (dark grey). Arrows on the right-hand axis indicate the respective temperature range from the core-top value to the minimum 200 yrs B.P. for each curve. This purpose is to illustrate the effects of changing the pre-exponential (B) and exponential (A) constants. Changing B primarily affects the position of the curve on the y-axis, where changing A affects the amplitude of the curve.

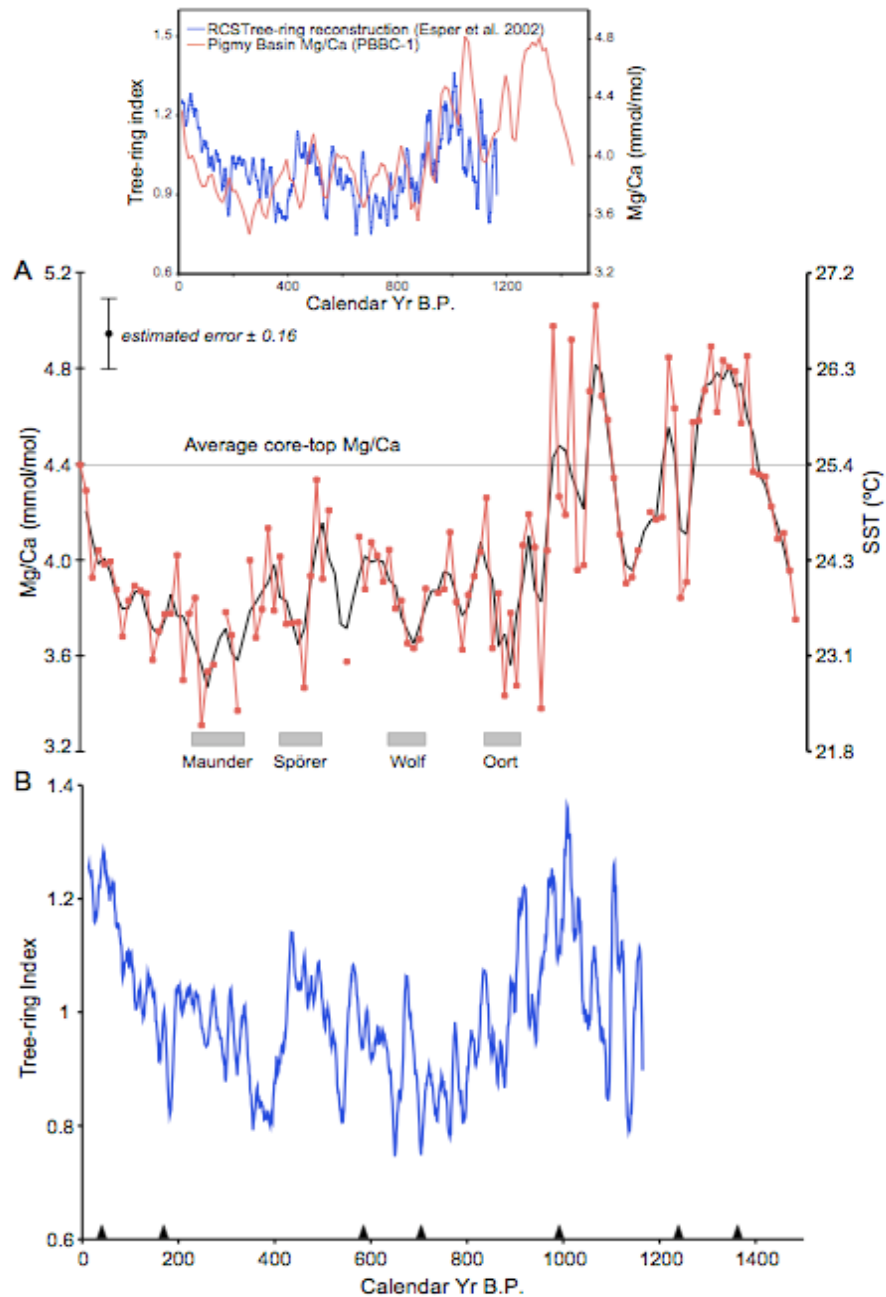


Figure 6. Mg/Ca-derived SST Record and Northern Hemisphere reconstruction. (A) Mg/Ca of *Globigerinoides ruber* (white variety) from core PBBC 1. The Mg/Ca record is plotted with the corresponding SST($^{\circ}$ C) values on the secondary axis. Markers indicate individual Mg/Ca measurements, and solid line is a 3-pt running mean. The overall precision of the Mg/Ca data is ± 0.16 mmol/mol. (B) RCS curve from Esper et al. (2002). Inset shows an over-plot of Mg/Ca curve from PBBC-1 and the RCS curve from Esper et al. (2002). Pigmy Basin and RCS records are plotted against their independent time-scales.

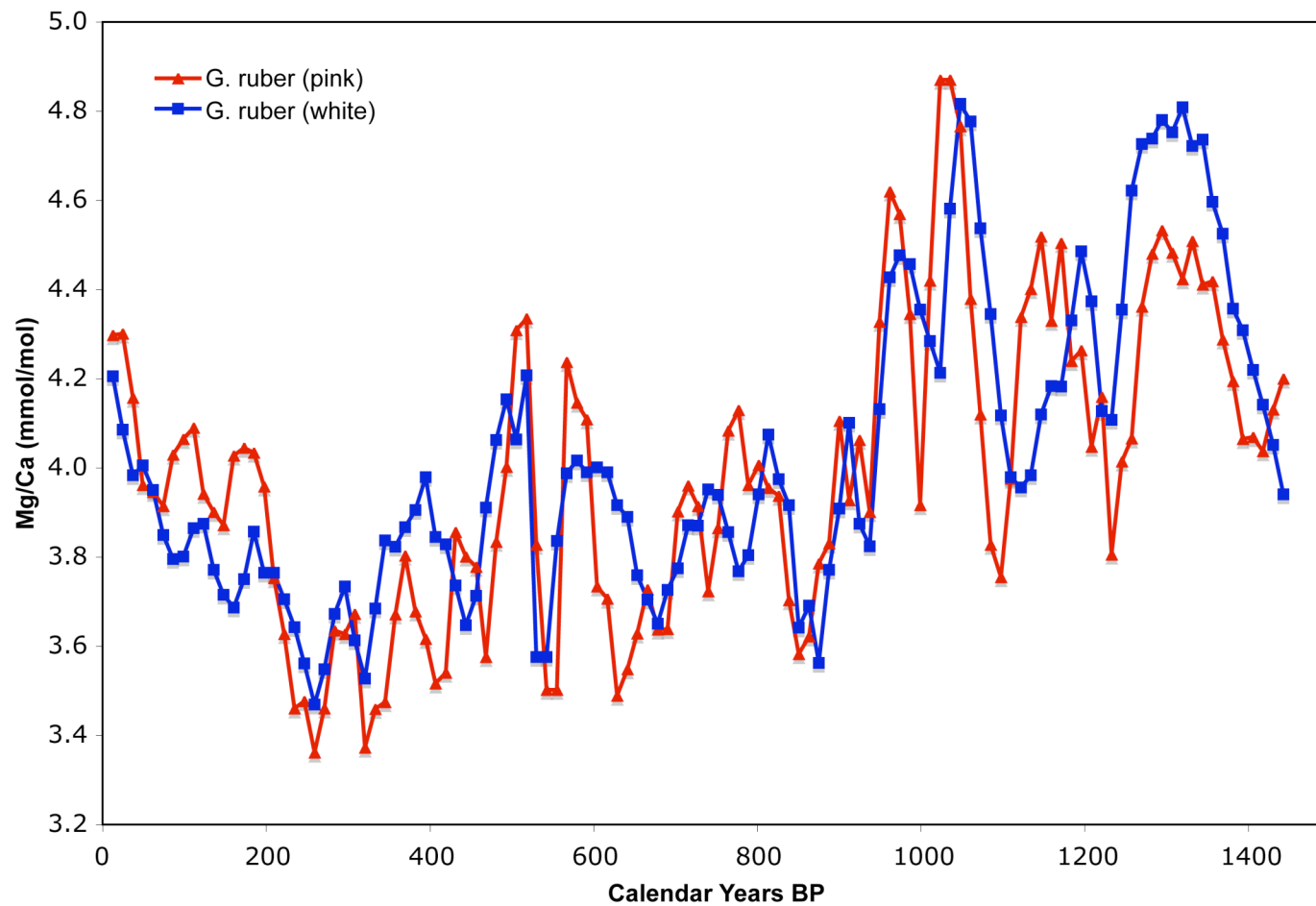


Figure 7. Overplot of raw Mg/Ca record from white and pink *G. ruber*. A 3-point running mean of the raw Mg/Ca values for *G. ruber* white (blue curve) and pink (red curve).

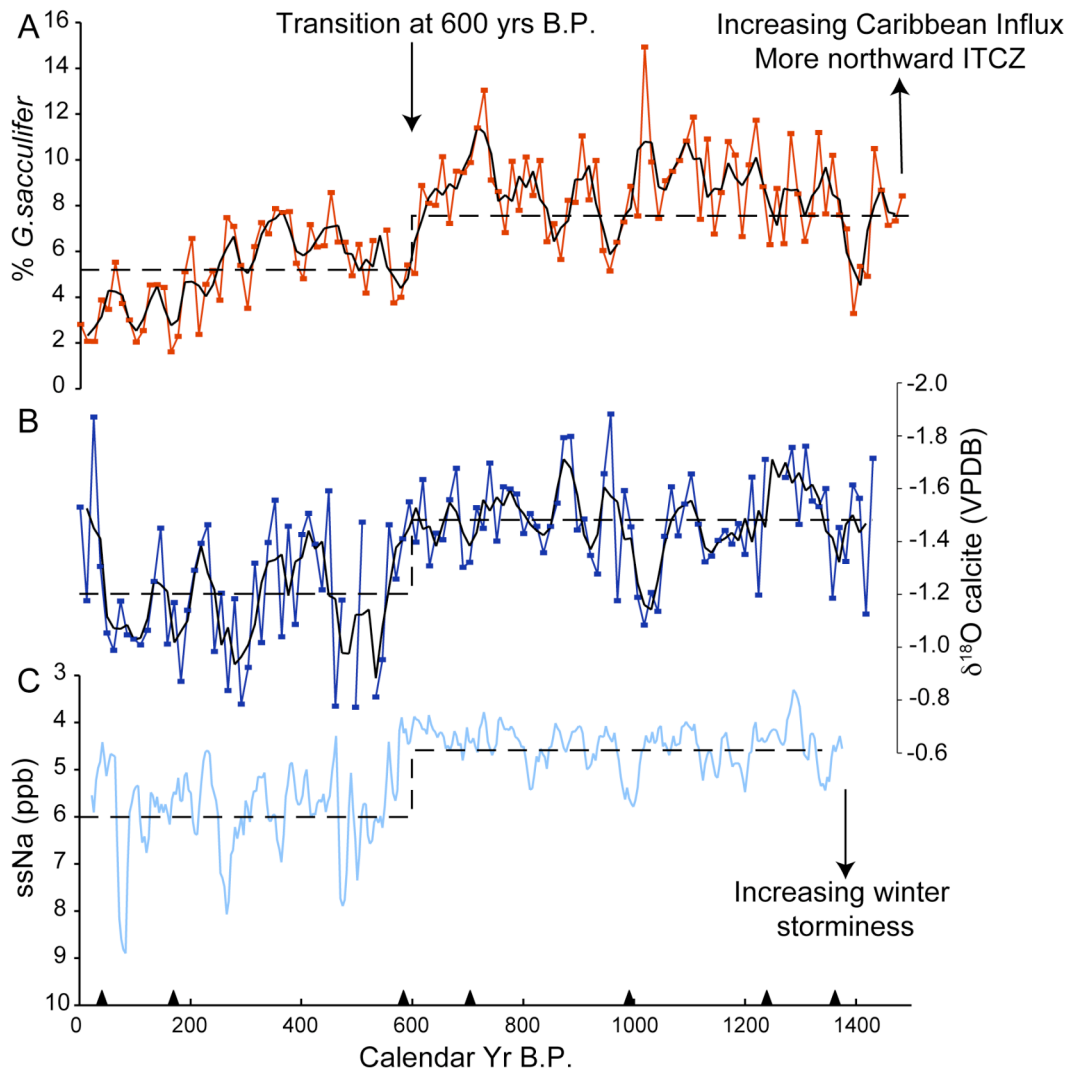


Figure 8. Pigmy Basin % *G. sacculifer*, $\delta^{18}\text{O}_{\text{calcite}}$ and GISP2 ssNa. (A) Relative abundance variations of the planktic foraminifer *Globigerinoides sacculifer* (B) and *G. ruber* (white variety) $\delta^{18}\text{O}$ measured in core PBBC-1 plotted against calibrated calendar yr B.P. Markers show individual measurements, while solid lines are 3-point running means. (C) Sea-salt-sodium (ssNa) record from GISP 2 ice core. The ssNa record is a 20 yr smoothed version, re-sampled at 6 yr resolution, and is plotted against the time scale for GISP2 (from Meeker and Mayewski, 2002).

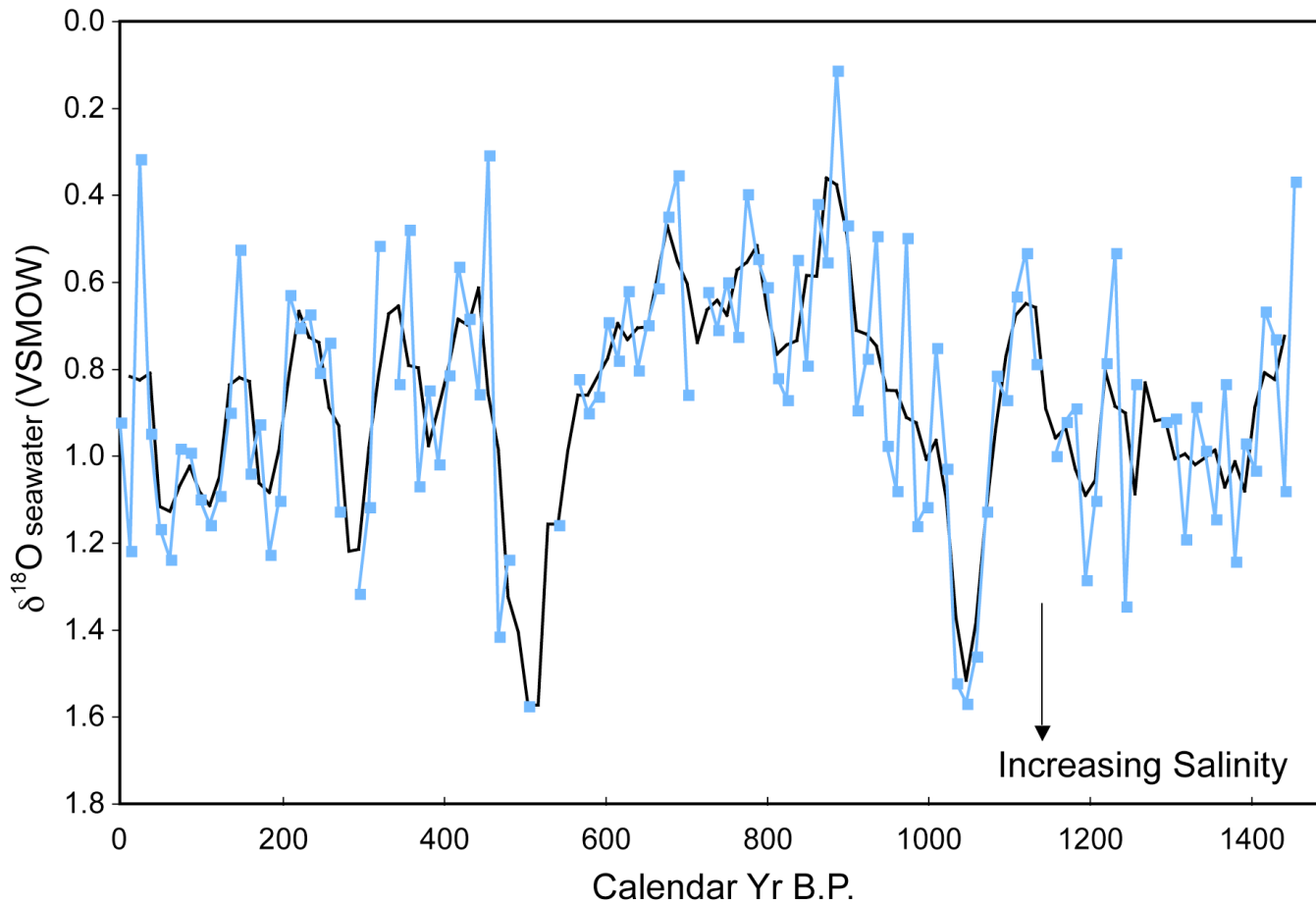


Figure 9. Calculated $\delta^{18}\text{O}_{\text{seawater}}$. Markers indicate individual values and 3-point running mean is shown in bold. $\delta^{18}\text{O}_{\text{seawater}}$ was calculated from paired Mg/Ca-SST estimates and $\delta^{18}\text{O}_{\text{calcite}}$ measurements using the equation for the planktonic foraminifer *Orbulina universa* (high-light) [$\text{SST}^{\circ}\text{C} = 14.9 - 4.8(\delta\text{c} - \delta\text{w})$] from Bemis et al. (1998). The resulting $\delta^{18}\text{O}_{\text{seawater}}$ is converted from VPDB to VSMOW by adding 0.27‰.

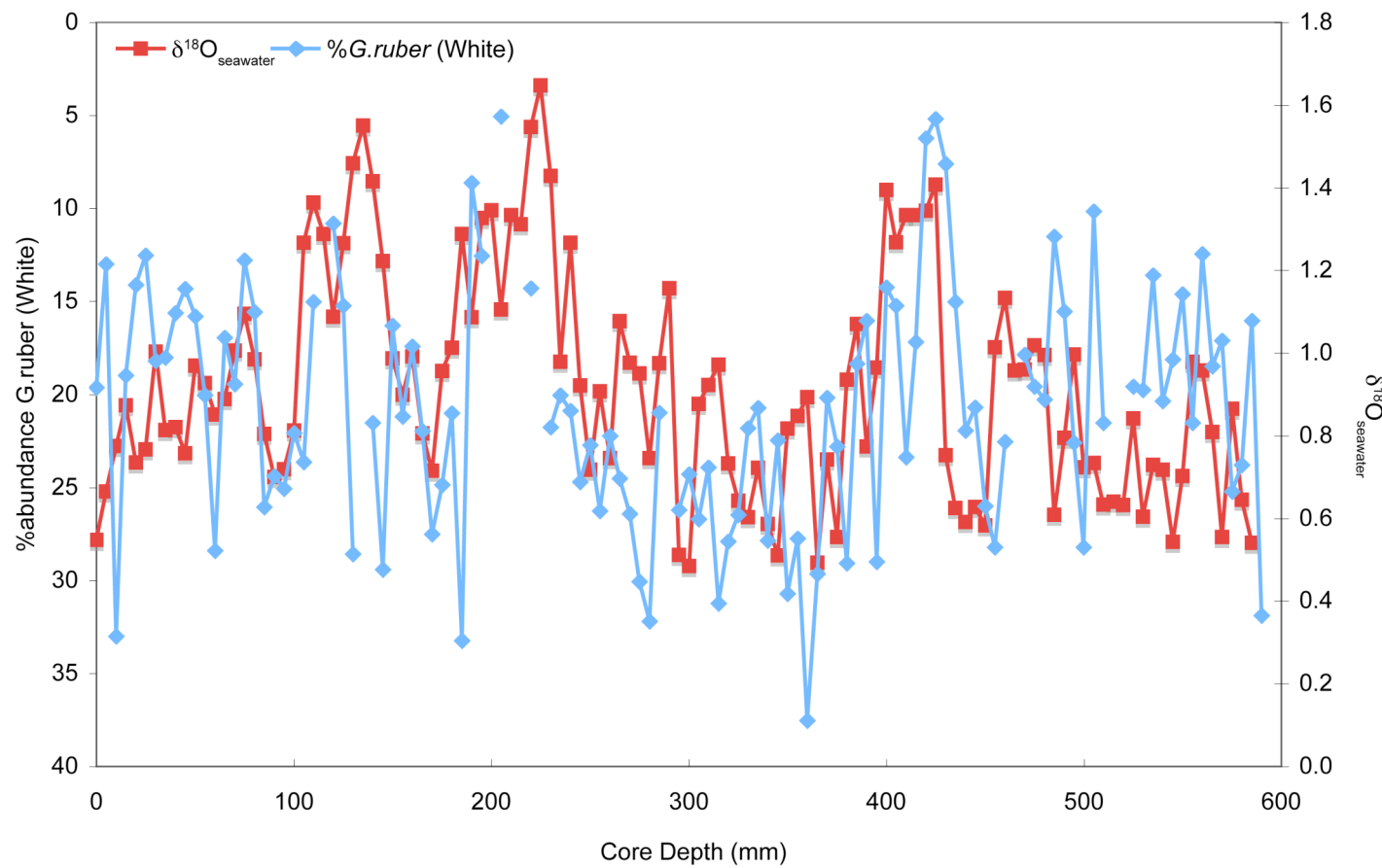


Figure 10. Comparison of $\delta^{18}\text{O}_{\text{seawater}}$ with % abundance *G. ruber* (white). The %abundance of white *G. ruber* (blue curve) is overplotted on the $\delta^{18}\text{O}_{\text{seawater}}$ record (red). Increasing $\delta^{18}\text{O}_{\text{seawater}}$ values are interpreted as increasing salinity. Note that the %abundance axis is plotted inversely, so that % abundance and $\delta^{18}\text{O}_{\text{seawater}}$ are anticorrelated.

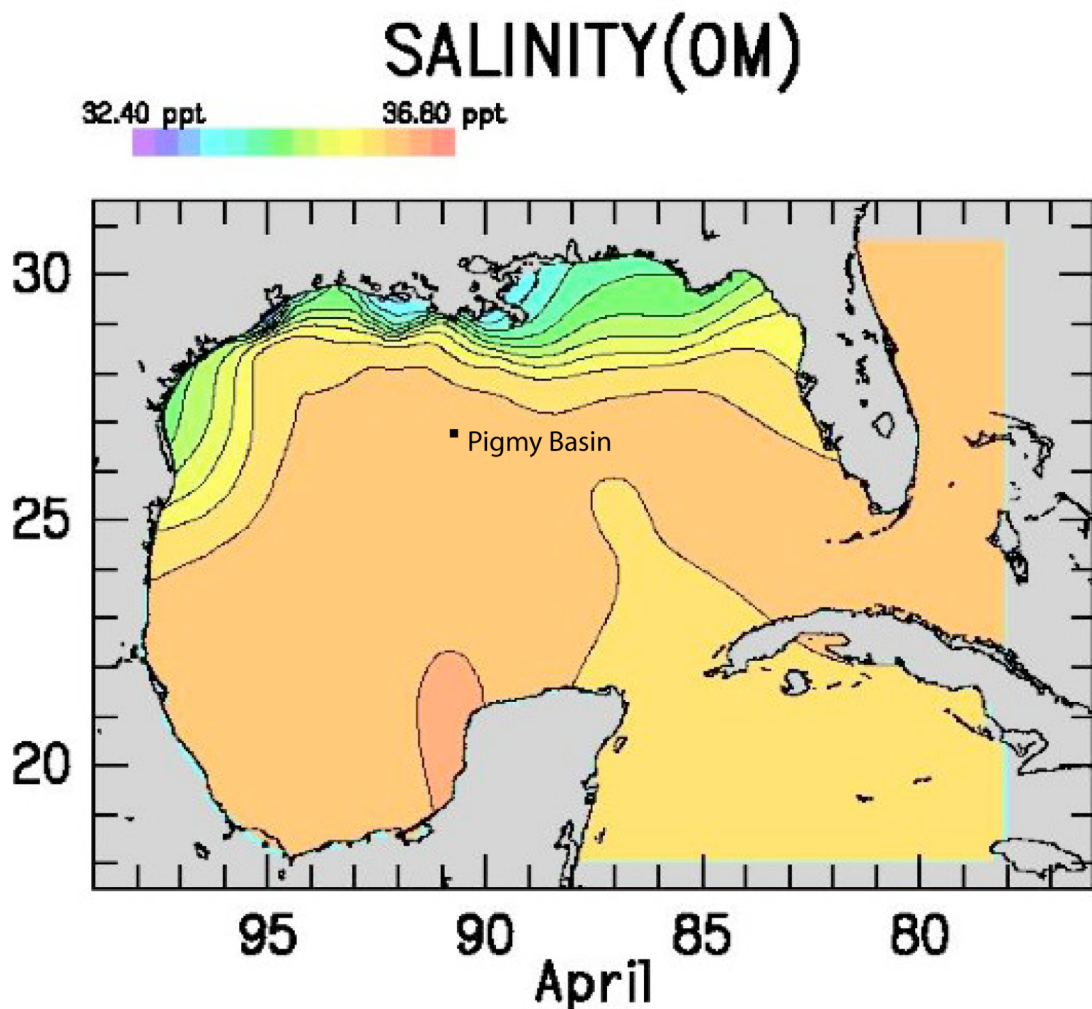


Figure 11. Model of Gulf of Mexico salinity during the month of April. This figure represents a surface salinity model for the GOM during for April, the month of maximum Mississippi River discharge. The model illustrates that even during maximum Mississippi River discharge, the surface salinity of the open GOM, over the Pigmy Basin, is not affected. (<http://www.dynalysis.com/Projects/gom/gom/images/main.htm>)

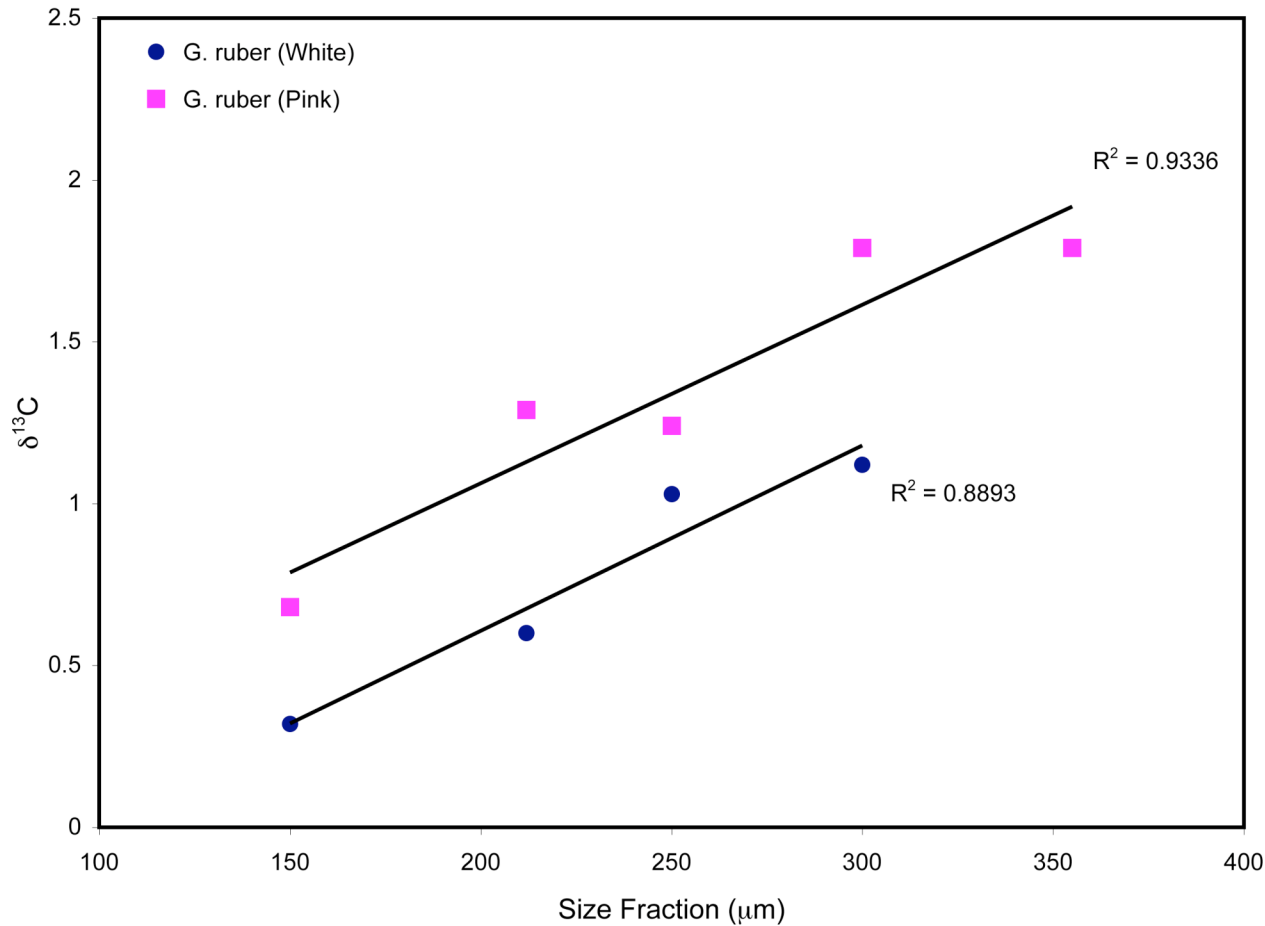


Figure 12. Size fraction versus $\delta^{13}\text{C}$ for white and pink *G. ruber*. $\delta^{13}\text{C}$ is plotted as a function of size for *G. ruber* white (circle) and *G. ruber* pink (square). X-axis values represent the low end of the size range (i.e. 150-212 μm is plotted as 150 μm). A least squares regression line and R^2 values are shown for both datasets

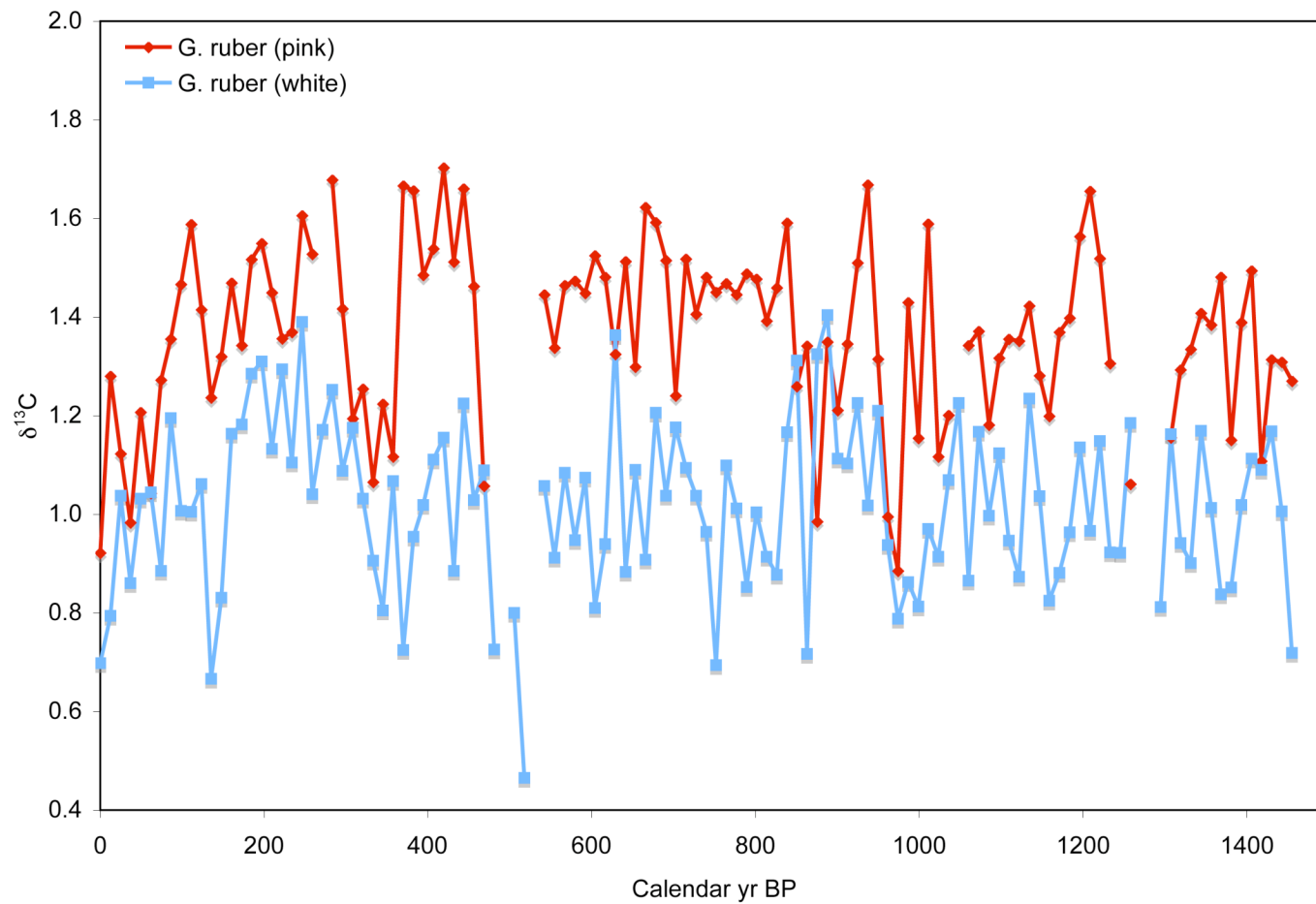


Figure 13. *G. ruber* $\delta^{13}\text{C}$ record (pink and white). Red curve represents raw $\delta^{13}\text{C}$ data for the 250-300 μm size fraction of pink *G. ruber* for core PBBC-1, and blue curve represents raw $\delta^{13}\text{C}$ data for the 250-300 μm size fraction of white *G. ruber*. The average difference was calculated between the 2 curves, and resulted in a 0.35‰ enrichment in pink *G. ruber* relative to white.

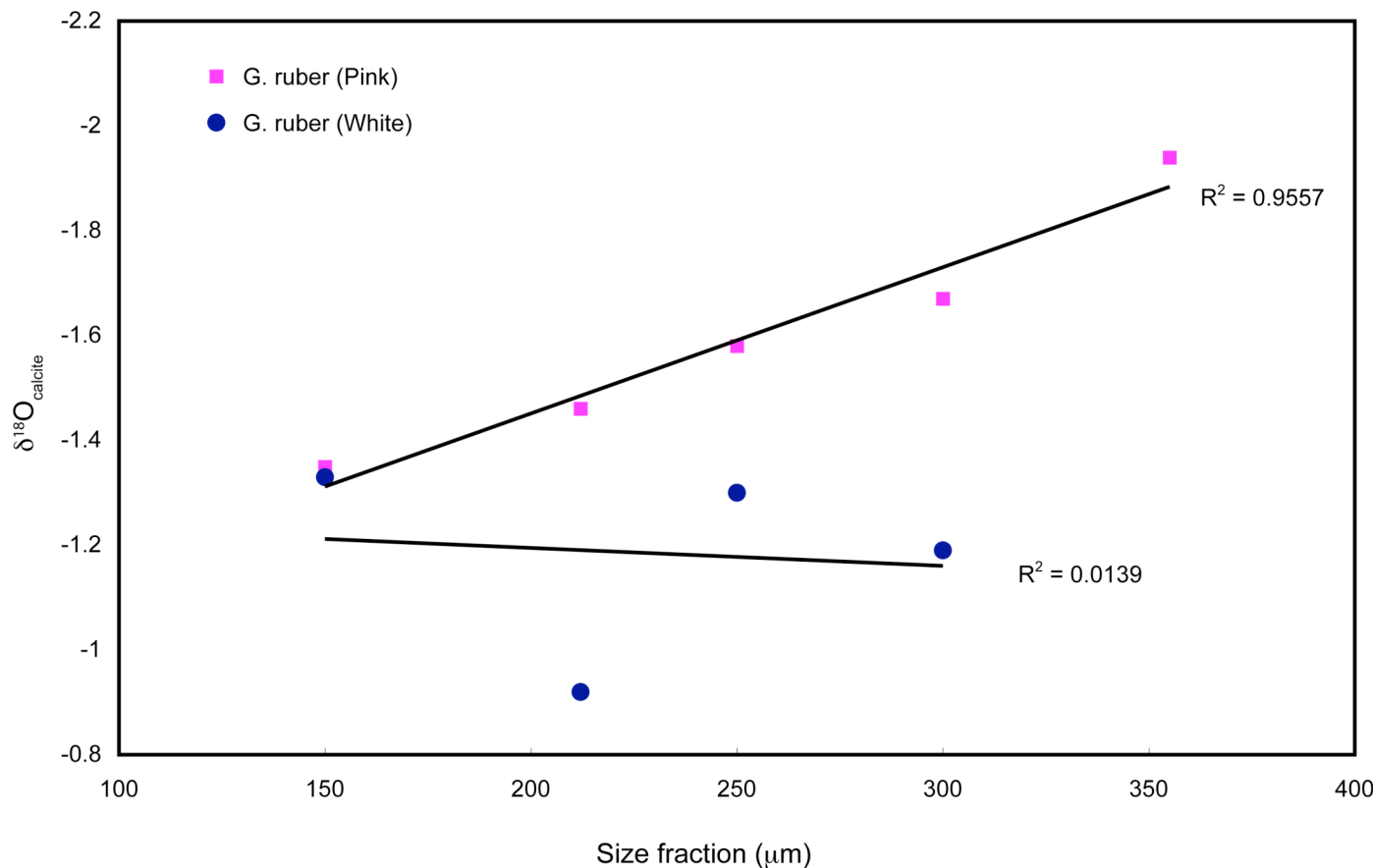


Figure 14. Size fraction versus $\delta^{18}\text{O}$ for white and pink *G. ruber*. $\delta^{18}\text{O}$ is plotted as a function of size for *G. ruber* pink (square) and *G. ruber* white (circle). Note that the Y-axis $\delta^{18}\text{O}$ values are plotted inversely. Least squares regression line and R^2 values are shown for both datasets.

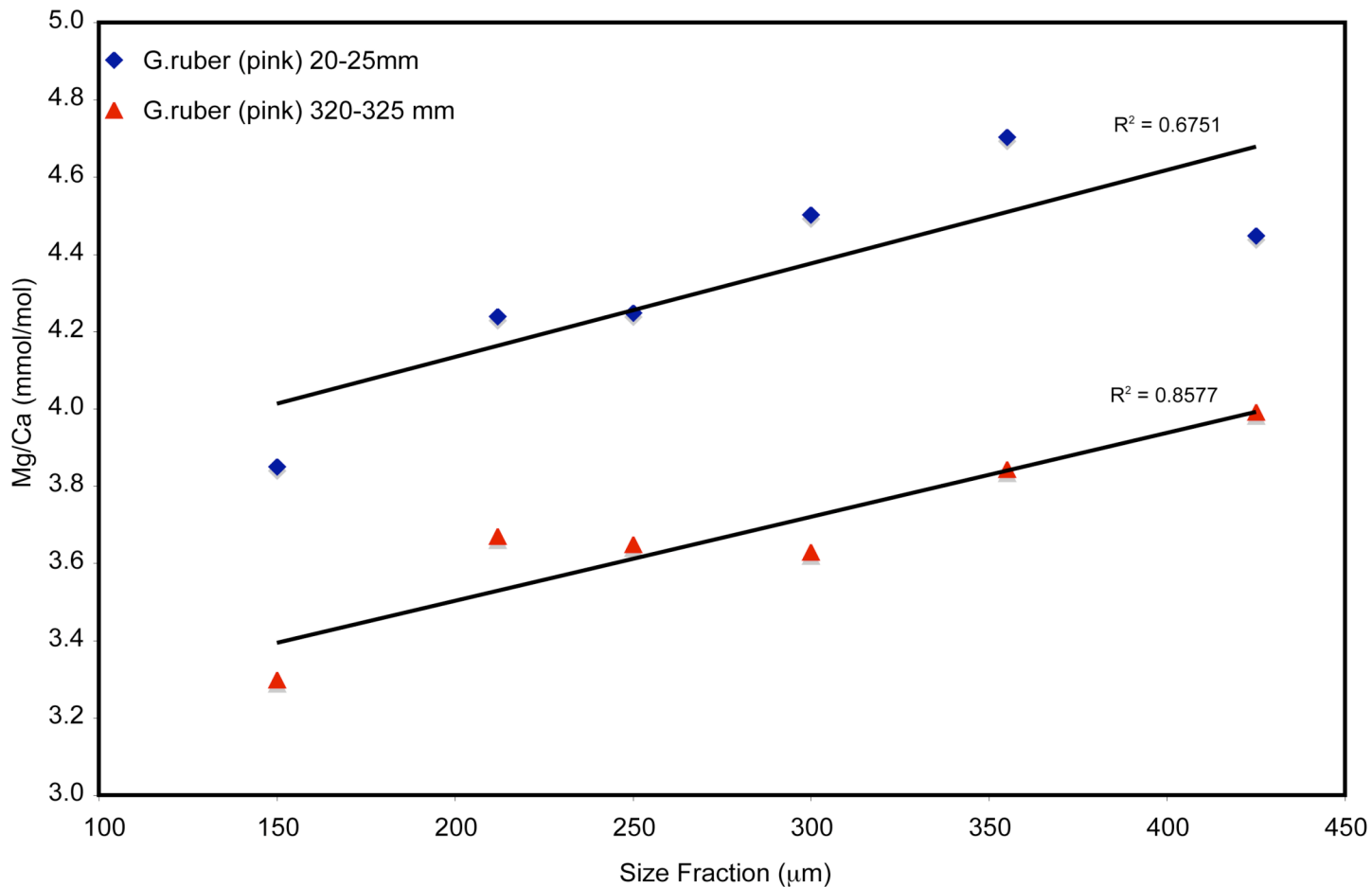


Figure 15. Size fraction versus Mg/Ca for *G. ruber* (pink). Data is shown for two different core-depths of Pigmy Basin box core PBBC-1, 20-25 mm (blue) and 320-325mm (red). Least squares regression lines are plotted with R^2 values.

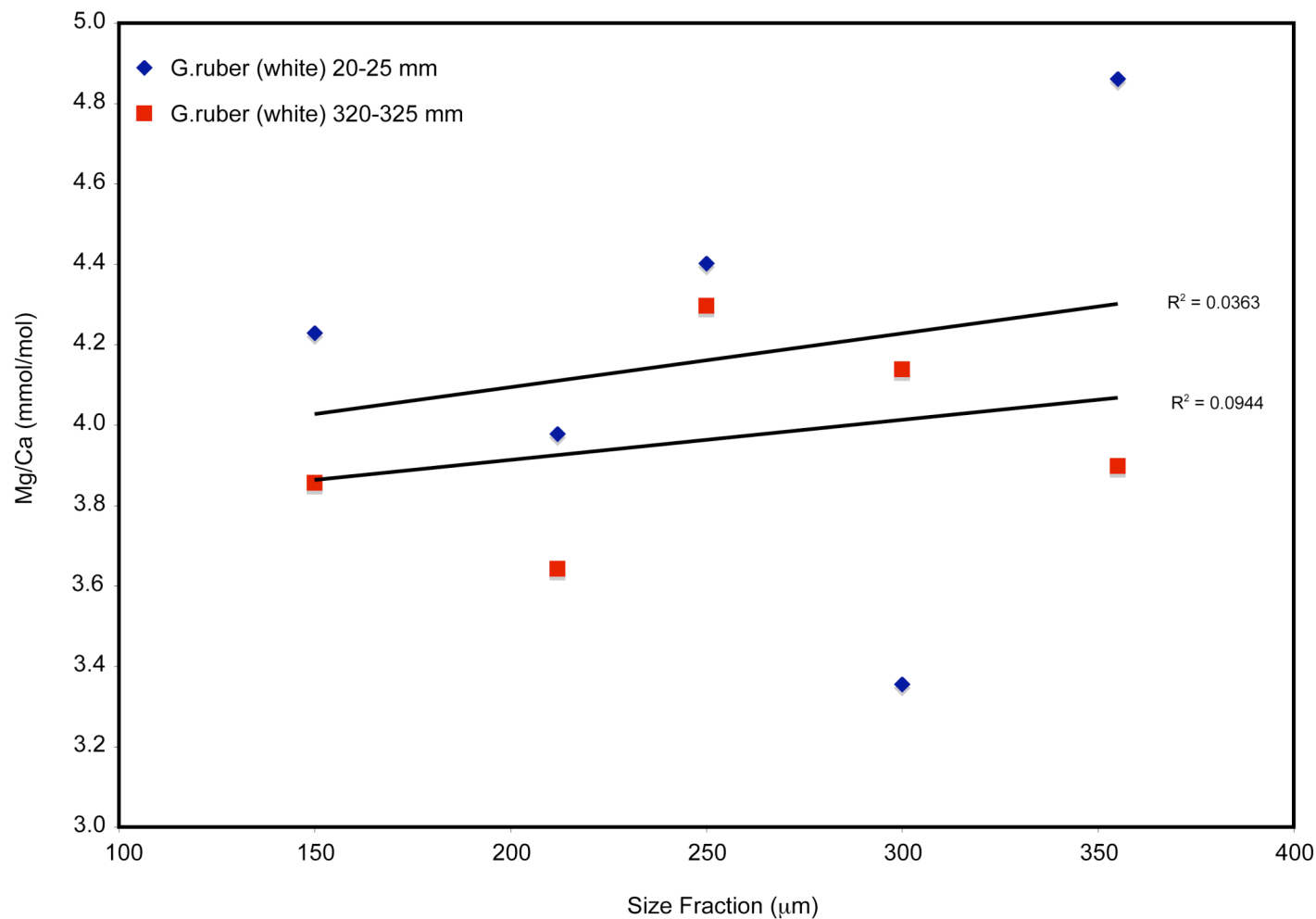


Figure 16. Size fraction versus Mg/Ca for *G. ruber* (white). Data is shown for two different core-depths of Pigmy Basin box core PBBC-1, 20-25 mm (blue) and 320-325mm (red). Least squares regression lines are plotted with R^2 values.

REFERENCES

- Anand, P., Elderfield, H., and Conte, M. H., 2003, Calibration of Mg/Ca thermometry in planktonic foraminifera from a sediment trap time series: *Paleoceanography*, v. 18, 1050, doi: 10.1029/2002PA000846.
- Barker, S., Greaves, M., Elderfield, H., 2003, A study of cleaning procedures used for foraminiferal Mg/Ca paleothermometry: *Geochemistry Geophysics Geosystems*, v. 4, doi: 10.1029/2003GC000559.
- Bemis, B.E., Spero, H.J., Bijma, J., and Lea, D.W., 1998, Reevaluation of the oxygen isotopic composition of planktonic foraminifera: Experimental results and revised paleotemperature equations: *Paleoceanography*, v. 13, p. 150–160.
- Berger, W. A., Killingley, J. S. and Vincent, E., 1978, Stable isotopes in deep sea carbonates: Box core ERDC-92, west equatorial Pacific: *Oceanologica Acta*, v. 1, p. 203-216.
- Broecker, W. S., 2001, Paleoclimate – Was the medieval warm period global?: *Science*, v. 291, p. 1497-1499.
- Bouma, A. H., and Coleman, J. M., 1986, Intraslope basin deposits and the potential relation to the continental shelf, northern Gulf of Mexico: *Transactions-Gulf Coast Association of Geological Societies*, v. XXXVI, p. 419-428.
- Bowen, G. L., and Revenaugh, J., 2003, Interpolating the isotopic composition of modern meteoric precipitation: *Water Resource Research*, v.39, doi:10.1029/2003WR002086.
- Boyle, E. A., and Keigwin, L. D., 1985, Comparison of Atlantic and Pacific paleochemical records for the Last 215,000 years: Changes in deep ocean circulation and chemical inventories: *Earth and Planetary Science Letters*, v. 76, p. 135–150.
- Crowley, T.J. and Lowery, T., 2000, How Warm was the Medieval Warm Period?: *Ambio*, v. 29, p. 51-54.
- Curry, W. B., and Matthews, R. K., 1981, Equilibrium ^{18}O fractionation in small size fraction planktic foraminifera: Evidence from recent Indian Ocean sediments: *Marine Micropaleontology*, v. 6, p. 327-337.

- Dekens, P. S., Lea, D. W., Pak, D. K., and Spero, H.J., 2002, Core top calibration of Mg/Ca in tropical foraminifera: Refining paleotemperature estimation: *Geochemistry, Geophysics, Geosystems*, v. 3, doi: 10.129/2001/GC000200.
- Deuser, W. G., 1987, Seasonal variations in isotopic composition and deep-water fluxes of the tests of perennially abundant planktonic foraminifera of the Sargasso Sea: Results from sediment-trap collections and their paleoceanographic significance: *Journal of Foraminiferal Research*, v. 17, p. 14 – 27.
- Elderfield, H., Vautravers, M., and Cooper, M. 2002, The relationship between shell size and Mg/Ca, Sr/Ca, d18O, and d13C of species of planktonic foraminifera: *Geochemistry Geophysics and Geosystems*, v. 3, doi: 10.1029/2001GC000194.
- Esper, J., Cook, E. R., and Schweingruber, F. H., 2002, Low-frequency signals in long tree-ring chronologies for reconstructing past temperature variability: *Science*, v. 295, p. 2250-2254.
- Fairbanks, R. G., Charles, C. D., Wright, J. D., 1992, Origin of Global Meltwater Pulses, Radiocarbon after Four Decades: An Interdisciplinary Perspective. R. E. Taylor et al. (eds) Springer-Verlag, New York.
- Flower, B. P., Hastings, D. W., Hill, H. W., Quinn, T. M., 2004, Phasing of deglacial warming and Laurentide Ice Sheet meltwater in the Gulf of Mexico: *Geology*, v. 32, p. 597-600.
- Giannini, A., Kushnir, Y., and Cane, M. A., 2000, Interannual variability of Caribbean rainfall, ENSO and the Atlantic Ocean: *Journal of Climate*, v. 13, p. 297-311.
- Goodkin, N. F., Hughen, K. A., Cohen, A. L., and Smith, S. R., 2005, Record of Little Ice Age sea surface temperatures at Bermuda using a growth-dependent calibration of coral Sr/Ca: *Paleoceanography*, v. 20, PA4016, doi: 10.1029/2005PA001140.
- Keigwin, L. D., 1996, The Little Ice Age and Medieval Warm Period in the Sargasso Sea: *Science*, v. 274, p. 1504-1508.
- Levitus, S., 2003, National Oceanographic Data Center World Ocean Atlas 1994, at <http://www.cdc.noaa.gov/>, Clim. Data Cent., Boulder, Colo.
- LoDico, J. M., B. P. Flower, and T. M. Quinn, 2006, Subcentennial-scale climatic and hydrologic variability in the Gulf of Mexico during the early Holocene: *Paleoceanography*, v. 21, PA3015, doi:10.1029/2005PA001243.
- Lund, D. C., and Curry W., 2006, Florida current surface temperature and salinity variability during the last millennium: *Paleoceanography*, v. 21, PA2009, doi: 10.1029/2005PAA001218.

- Mann, M. E., and Jones, P. D., 2003, Global surface temperature over the past two millennia: *Geophysical Research Letters*, v. 30, p. 1820-1823.
- McConaughey, T. A., 2003, Sub-equilibrium oxygen-18 and carbon-13 levels in biological carbonates: carbonate and kinetic models: *Coral Reefs*, v. 22, p. 316-327.
- Meeker L. D., Mayewski, P.A., 2002, A 1400-year high-resolution record of atmospheric circulation over the North Atlantic and Asia: *The Holocene*, v. 12, p. 257-266.
- Moberg, A., Sonechkin, D., M., Holmgren, K., Datsenko, N., M., and Karlén, W., 2005, Highly variable Northern Hemisphere temperatures reconstructed from low- and high-resolution proxy data: *Nature*, v. 433, p. 613-617.
- Newton, A., Thunell, R., and Stott, L., 2006, Climate and hydrographic variability in the Indo-Pacific Warm Pool during the last millennium: *Geophysical Research Letters*, v. 33, p. L19710, doi: 10.1029/2006GL027234.
- Ortner, P. B., Lee, T. N., Milne, P. J., Zika, R. G., Clarke, M. E., Podesta, G. P., Swart, P. K., Tester, P. A., Atkinson, L. P., Johnson, W. R., 1995, Mississippi River flood waters that reached the Gulf Stream: *Journal of Geophysical Research*, v. 100, p. 595-601.
- Pena, L. D., Calvo, E., Cacho, I., Eggins, S., and Pelejero, C., 2005, Identification and removal of Mn-Mg-rich contaminant phases on foraminiferal tests: Implications for Mg/Ca past temperature reconstructions: *Geochemistry, Geophysics, Geosystems*, v. 6, Q09P02, doi:10.1029/2005GC000930.
- Poore, R. Z., Quinn, T. M., and Verardo, S., 2004, Century-scale movement of the Atlantic Intertropical Convergence Zone linked to solar variability: *Geophysical Research Letters*, v. 31, L12214, doi: 10.1029/2004GL019940.
- Ravelo, A., C., and Fairbanks, R., G., 1995, Carbon isotopic fractionation in multiple species of planktonic foraminifera from core-tops in the tropical Atlantic: *Journal of Foraminiferal Research*, v. 25, p.53-74.
- Schmitt, R. W., Bogden, P. S., Dorman, C. E., 1989, Evaporation minus precipitation and density fluxes for the North Atlantic: *Journal of Physical Oceanography*, v. 19, p. 1208-1221.
- Stuiver, M., Reimer, P. J., Bard, E., Beck, J.W., Burr, G. S., Hughen, K. A., Kromer, B., McCormac, F. G., Van Der Plicht, J., and Spurk M., 1998, INTCAL98 radiocarbon age calibration 24,000–0 cal BP: *Radiocarbon*, v. 40, p. 1041–1083.

Watanabe, T., Winter, A. and Oba, T., 2001, Seasonal changes in sea surface temperature and salinity during the Little Ice Age in the Caribbean Sea deduced from Mg/Ca and $^{18}\text{O}/^{16}\text{O}$ ratios in corals: *Marine Geology*, v. 173, p. 21-35.

Wang, C., and Enfield, C. B., 2001, The tropical Western Hemisphere Warm Pool: *Geophysical Research Letters*, v. 28, p. 1635-1638.

Williams, D. F., Be, A. W. H., and Fairbanks, R. G., 1981, Seasonal stable isotopic variations in living planktonic foraminifera from Bermuda plankton tows: *Paleogeography, Paleoclimatology, Paleoecology*, v. 33, p. 71-102.

Winter, A., Ishioroshi, H., Watanabe, T., Oba, T., and Christy, J., 2000, Caribbean Sea surface temperatures: Two-to-three degrees cooler than present during the Little Ice Age: *Geophysical Research Letters*, v. 27, p. 3365-3368.

APPENDICES

Appendix I. Data Table for white *G. ruber*

Cal Yr BP	Depth (mm)	Mg/Ca (mmol/mol)	SST (°C)	$\delta^{18}\text{O}(\text{calcite})$	$\delta^{18}\text{O}(\text{sw})$	$\delta^{13}\text{C}$
0.0	0	4.398	25.35	-1.530	0.92	0.70
12.3	5	4.290	25.08	-1.175	1.22	0.79
24.7	10	3.927	24.10	-1.871	0.32	1.04
37.0	15	4.040	24.41	-1.305	0.95	0.86
49.3	20	3.983	24.25	-1.053	1.17	1.03
61.7	25	3.993	24.28	-0.988	1.24	1.05
74.0	30	3.876	23.95	-1.174	0.98	0.89
86.3	35	3.681	23.38	-1.046	0.99	1.19
98.7	40	3.831	23.82	-1.031	1.10	1.01
111.0	45	3.892	24.00	-1.009	1.16	1.01
123.3	50	3.872	23.94	-1.064	1.09	1.06
135.7	55	3.860	23.91	-1.248	0.90	0.67
148.0	60	3.583	23.08	-1.451	0.52	0.83
160.3	65	3.703	23.44	-1.012	1.04	1.16
172.7	70	3.774	23.65	-1.169	0.93	1.18
185.0	75	3.777	23.66	-0.871	1.22	1.29
197.3	80	4.020	24.35	-1.140	1.10	1.31
209.7	85	3.498	22.81	-1.291	0.63	1.13
222.0	90	3.777	23.66	-1.392	0.70	1.29
234.3	95	3.841	23.85	-1.463	0.67	1.11
246.7	100	3.310	22.20	-0.983	0.81	1.39
259.0	105	3.533	22.92	-1.204	0.74	1.04
271.3	110	3.563	23.02	-0.836	1.12	1.17
283.7	115			-1.183		1.25
296.0	120	3.782	23.68	-0.785	1.31	1.09
308.3	125	3.685	23.39	-0.923	1.12	1.18
320.7	130	3.371	22.40	-1.318	0.51	1.03
333.0	135			-1.017		0.91
345.3	140	3.998	24.30	-1.396	0.83	0.81
357.7	145	3.675	23.36	-1.556	0.48	1.07

Appendix I. Data Table for white *G. ruber* (continued)

Cal Yr BP	Depth (mm)	Mg/Ca (mmol/mol)	SST (°C)	$\delta^{18}\text{O}(\text{calcite})$	$\delta^{18}\text{O}(\text{sw})$	$\delta^{13}\text{C}$
370.0	150	3.794	23.71	-1.040	1.07	0.72
382.3	155	4.133	24.66	-1.458	0.85	0.95
394.7	160	3.789	23.70	-1.086	1.02	1.02
407.0	165	4.015	24.34	-1.425	0.81	1.11
419.3	170	3.733	23.53	-1.506	0.56	1.16
431.7	175	3.737	23.55	-1.390	0.68	0.88
444.0	180	3.739	23.55	-1.217	0.86	1.22
456.3	185	3.466	22.71	-1.592	0.31	1.03
468.7	190	3.933	24.11	-0.777	1.41	1.09
481.0	195	4.335	25.19	-1.178	1.24	0.73
493.3	200	3.921	24.08			
505.7	205	4.208	24.86	-0.773	1.57	0.80
518.0	210			-1.473		0.47
530.3	215					
542.7	220	3.575	23.05	-0.812	1.16	1.06
555.0	225			-0.952		0.91
567.3	230	4.098	24.57	-1.463	0.82	1.08
579.7	235	3.878	23.95	-1.258	0.90	0.95
592.0	240	4.075	24.51	-1.410	0.86	1.07
604.3	245	4.019	24.35	-1.550	0.69	0.81
616.7	250	3.909	24.05	-1.398	0.78	0.94
629.0	255	4.042	24.42	-1.634	0.62	1.36
641.3	260	3.797	23.72	-1.307	0.80	0.88
653.6	265	3.830	23.82	-1.432	0.70	1.09
666.0	270	3.652	23.29	-1.406	0.61	0.91
678.3	275	3.631	23.22	-1.557	0.45	1.21
690.6	280	3.668	23.34	-1.677	0.35	1.04
703.0	285	3.880	23.96	-1.302	0.86	1.18
715.3	290			-1.321		1.09
727.6	295	3.863	23.91	-1.528	0.62	1.04

Appendix I. Data Table for white *G. ruber* (continued)

Cal Yr BP	Depth (mm)	Mg/Ca (mmol/mol)	SST (°C)	$\delta^{18}\text{O}(\text{calcite})$	$\delta^{18}\text{O}(\text{sw})$	$\delta^{13}\text{C}$
740.0	300	3.878	23.96	-1.449	0.71	0.96
752.3	305	4.116	24.62	-1.696	0.60	0.69
764.6	310	3.825	23.80	-1.401	0.72	1.10
777.0	315	3.626	23.21	-1.606	0.39	1.01
789.3	320	3.854	23.89	-1.598	0.54	0.85
801.6	325	3.933	24.11	-1.580	0.61	1.00
814.0	330	4.034	24.39	-1.430	0.82	0.91
826.3	335	4.259	25.00	-1.505	0.87	0.88
838.6	340	3.631	23.22	-1.458	0.55	1.17
851.0	345	3.861	23.91	-1.357	0.79	1.31
863.3	350	3.433	22.60	-1.457	0.42	0.72
875.6	355	3.778	23.67	-1.545	0.55	1.33
888.0	360	3.476	22.74	-1.792	0.11	1.40
900.3	365	4.061	24.47	-1.797	0.47	1.11
912.6	370	4.190	24.82	-1.444	0.89	1.10
925.0	375	4.053	24.45	-1.485	0.77	1.23
937.3	380	3.380	22.43	-1.347	0.49	1.02
949.6	385	4.039	24.41	-1.277	0.97	1.21
962.0	390	4.977	26.73	-1.656	1.08	0.94
974.3	395	4.265	25.01	-1.881	0.50	0.79
986.6	400	4.188	24.81	-1.176	1.16	0.86
999.0	405	4.919	26.60	-1.592	1.12	0.81
1011.3	410	3.957	24.18	-1.455	0.75	0.97
1023.6	415	3.977	24.24	-1.189	1.03	0.91
1036.0	420	4.706	26.11	-1.084	1.52	1.07
1048.3	425	5.062	26.92	-1.207	1.57	1.23
1060.6	430	4.684	26.05	-1.135	1.46	0.86
1073.0	435	4.585	25.82	-1.419	1.12	1.17
1085.3	440	4.343	25.22	-1.607	0.81	1.00
1097.6	445	4.107	24.59	-1.421	0.87	1.12

Appendix I. Data Table for white *G. ruber* (continued)

Cal Yr BP	Depth (mm)	Mg/Ca (mmol/mol)	SST (°C)	$\delta^{18}\text{O}(\text{calcite})$	$\delta^{18}\text{O}(\text{sw})$	$\delta^{13}\text{C}$
1110.0	450	3.903	24.03	-1.542	0.63	0.95
1122.3	455	3.928	24.10	-1.655	0.53	0.87
1134.6	460	4.039	24.41	-1.465	0.79	1.23
1147.0	465			-1.322		1.04
1159.3	470	4.200	24.84	-1.344	1.00	0.83
1171.6	475	4.168	24.76	-1.404	0.92	0.88
1184.0	480	4.178	24.79	-1.442	0.89	0.96
1196.3	485	4.847	26.43	-1.390	1.28	1.14
1208.6	490	4.633	25.93	-1.468	1.10	0.97
1221.0	495	3.841	23.85	-1.351	0.78	1.15
1233.3	500	3.907	24.04	-1.644	0.53	0.92
1245.6	505	4.576	25.79	-1.197	1.34	0.92
1258.0	510	4.581	25.81	-1.711	0.83	1.18
1270.3	515	4.708	26.11			
1282.6	520	4.891	26.53			
1295.0	525	4.618	25.90	-1.642	0.92	0.81
1307.3	530	4.833	26.40	-1.755	0.91	1.16
1319.6	535	4.806	26.34	-1.464	1.19	0.94
1332.0	540	4.787	26.30	-1.760	0.88	0.90
1344.3	545	4.572	25.78	-1.553	0.99	1.17
1356.6	550	4.851	26.44	-1.532	1.14	1.01
1369.0	555	4.368	25.28	-1.600	0.83	0.84
1381.3	560	4.356	25.25	-1.186	1.24	0.85
1393.6	565	4.348	25.23	-1.453	0.97	1.02
1406.0	570	4.224	24.91	-1.324	1.03	1.11
1418.3	575	4.088	24.54	-1.614	0.67	1.09
1430.6	580	4.112	24.61	-1.563	0.73	1.17
1443.0	585	3.956	24.18	-1.125	1.08	1.01
1455.3	590	3.752	23.59	-1.714	0.37	0.72

Appendix II. Data Table for pink *G. ruber*

Cal Yr BP	Depth (mm)	Mg/Ca (mmol/mol)	$\delta^{18}\text{O}$ (calcite)	$\delta^{13}\text{C}$
0.0	0	4.048	-1.43	0.92
12.3	5	4.433	-1.12	1.28
24.7	10	4.413	-1.71	1.12
37.0	15	4.057	-1.27	0.98
49.3	20	4.002	-1.53	1.21
61.7	25	3.827	-1.61	1.04
74.0	30	4.008	-1.16	1.27
86.3	35	3.909	-1.68	1.36
98.7	40	4.171	-1.84	1.47
111.0	45	4.116	-1.44	1.59
123.3	50	3.983	-1.54	1.41
135.7	55	3.727	-1.61	1.24
148.0	60	3.992	-1.43	1.32
160.3	65	3.895	-1.48	1.47
172.7	70	4.195	-1.65	1.34
185.0	75	4.046	-1.37	1.52
197.3	80	3.862	-1.34	1.55
209.7	85	3.965	-1.39	1.45
222.0	90	3.430	-1.47	1.36
234.3	95	3.488	-1.69	1.37
246.7	100	3.465	-1.56	1.61
259.0	105		-1.63	1.53
271.3	110	3.259		
283.7	115	3.662	-1.41	1.68
296.0	120	3.986	-1.63	1.42
308.3	125	3.235	-1.28	1.19
320.7	130	3.795	-1.30	1.25
333.0	135	3.087	-1.18	1.06
345.3	140	3.495	-1.29	1.22
357.7	145	3.843	-1.27	1.12

Appendix II. Data Table for pink *G. ruber* (continued)

Cal Yr BP	Depth (mm)	Mg/Ca (mmol/mol)	$\delta^{18}\text{O}$ (calcite)	$\delta^{13}\text{C}$
370.0	150	3.675	-1.49	1.67
382.3	155	3.891	-1.62	1.66
394.7	160	3.468	-1.44	1.48
407.0	165	3.492	-1.24	1.54
419.3	170	3.591	-1.52	1.70
431.7	175		-1.34	1.51
444.0	180	4.122	-1.63	1.66
456.3	185	3.481	-1.15	1.46
468.7	190	3.730	-1.08	1.06
481.0	195	3.518		
493.3	200	4.256		
505.7	205	4.233		
518.0	210	4.437		
530.3	215			
542.7	220	3.219	-1.69	1.45
555.0	225	3.787	-1.42	1.34
567.3	230		-1.68	1.46
579.7	235	4.688	-1.42	1.47
592.0	240	3.604	-1.74	1.45
604.3	245	4.033	-1.65	1.53
616.7	250	3.566	-1.50	1.48
629.0	255	3.522	-1.58	1.33
641.3	260	3.380	-1.58	1.51
653.6	265	3.744	-1.80	1.30
666.0	270	3.761	-1.53	1.62
678.3	275	3.677	-1.81	1.59
690.6	280	3.474	-1.62	1.51
703.0	285	3.764	-1.54	1.24
715.3	290	4.470	-1.50	1.52
727.6	295	3.646	-1.69	1.41

Appendix II. Data Table for pink *G. ruber* (continued)

Cal Yr BP	Depth (mm)	Mg/Ca (mmol/mol)	$\delta^{18}\text{O}$ (calcite)	$\delta^{13}\text{C}$
740.0	300	3.628	-1.38	1.48
752.3	305	3.897	-1.41	1.45
764.6	310	4.071	-1.40	1.47
777.0	315	4.284	-1.50	1.45
789.3	320	4.036	-1.38	1.49
801.6	325	3.564	-1.46	1.48
814.0	330	4.420	-1.46	1.39
826.3	335	3.882	-1.41	1.46
838.6	340	3.511	-1.54	1.59
851.0	345	3.717	-1.59	1.26
863.3	350	3.520	-1.47	1.34
875.6	355	3.630	-1.60	0.98
888.0	360	4.207	-1.44	1.35
900.3	365	3.655	-1.49	1.21
912.6	370	4.455	-1.49	1.35
925.0	375	3.670	-1.54	1.51
937.3	380		-1.51	1.67
949.6	385	4.131	-1.71	1.31
962.0	390	4.525	-1.87	0.99
974.3	395	5.203	-1.46	0.89
986.6	400	3.980	-1.56	1.43
999.0	405	3.854	-1.23	1.15
1011.3	410		-1.52	1.59
1023.6	415	4.985	-1.43	1.12
1036.0	420	4.755	-1.51	1.20
1048.3	425		-2.02	-0.55
1060.6	430	4.776	-1.59	1.34
1073.0	435	3.981	-1.81	1.37
1085.3	440	3.601	-1.39	1.18
1097.6	445	3.899	-1.43	1.32

Appendix II. Data Table for pink *G. ruber* (continued)

Cal Yr BP	Depth (mm)	Mg/Ca (mmol/mol)	$\delta^{18}\text{O}$ (calcite)	$\delta^{13}\text{C}$
1110.0	450	3.763	-1.49	1.36
1122.3	455	4.264	-1.82	1.35
1134.6	460	4.987	-1.54	1.42
1147.0	465	3.952	-1.43	1.28
1159.3	470	4.619	-1.70	1.20
1171.6	475	4.418	-1.47	1.37
1184.0	480	4.477	-1.48	1.40
1196.3	485	3.823	-1.48	1.56
1208.6	490	4.493	-1.93	1.66
1221.0	495	3.827	-1.67	1.52
1233.3	500		-1.66	1.31
1245.6	505	3.783		
1258.0	510	4.245	-1.39	1.06
1270.3	515	4.170		
1282.6	520	4.670		
1295.0	525	4.601		
1307.3	530	4.327	-1.93	1.16
1319.6	535	4.520	-1.63	1.29
1332.0	540		-1.60	1.33
1344.3	545	4.498	-1.59	1.41
1356.6	550	4.324	-1.72	1.38
1369.0	555	4.435	-1.48	1.48
1381.3	560	4.104	-1.64	1.15
1393.6	565	4.044	-1.61	1.39
1406.0	570	4.046	-1.45	1.49
1418.3	575	4.117	-1.66	1.11
1430.6	580	3.949	-1.61	1.31
1443.0	585	4.328	-1.57	1.31
1455.3	590	4.325	-1.66	1.27

Appendix III. Faunal abundance for 5 common planktic foraminifers

Cal Yr BP	Core Depth (mm)	<i>G. sacculifer</i> (%)	<i>G. ruber</i> pk (%)	<i>G. ruber</i> wht (%)	<i>N. dutertrei</i> (%)
0.0	0	2.8	17.2	27.8	7.5
12.3	5	2.1	17.8	25.2	9.5
24.7	10	2.1	18.0	22.8	7.4
37.0	15	3.9	12.2	20.6	9.3
49.3	20	3.5	15.1	23.7	7.3
61.7	25	5.5	11.9	23.0	6.7
74.0	30	3.7	11.8	17.7	5.3
86.3	35	3.0	13.2	21.9	7.8
98.7	40	2.0	6.1	21.8	7.8
111.0	45	2.5	7.6	23.2	10.5
123.3	50	4.5	9.7	18.4	6.5
135.7	55	4.5	10.0	19.4	9.4
148.0	60	4.4	12.9	21.1	7.1
160.3	65	1.6	10.9	20.3	7.1
172.7	70	2.3	13.1	17.6	6.9
185.0	75	5.1	13.4	15.7	5.8
197.3	80	6.6	12.2	18.1	5.9
209.7	85	2.4	11.2	22.1	7.5
222.0	90	4.6	8.5	24.4	8.5
234.3	95	5.2	11.9	24.0	10.9
246.7	100	3.9	9.7	21.9	14.2
259.0	105	7.5	7.5	11.8	14.6
271.3	110				
283.7	115	7.1	3.2	9.7	15.5
296.0	120	5.4	7.8	11.4	12.6
308.3	125	3.5	5.3	15.8	12.6
320.7	130	6.2	6.5	11.9	15.8
333.0	135	7.3	5.0	7.6	13.2
345.3	140	6.8	7.1	5.5	15.4
357.7	145	7.9	4.9	8.5	13.4

Appendix III. Faunal abundance for 5 common planktic foraminifers (continued)

Cal Yr BP	Core Depth (mm)	<i>G. sacculifer</i> (%)	<i>G. ruber</i> pk (%)	<i>G. ruber</i> wht (%)	<i>N. dutertrei</i> (%)
370.0	150	7.7	8.0	12.8	9.6
382.3	155	7.7	11.9	18.1	7.1
394.7	160	5.5	15.8	20.0	6.8
407.0	165	4.8	16.3	17.9	6.4
419.3	170	7.2	16.7	22.1	8.4
431.7	175	6.2	7.5	24.1	12.1
444.0	180	6.3	8.0	18.8	10.7
456.3	185	8.6	7.1	17.5	10.4
468.7	190	6.4	5.8	11.4	13.4
481.0	195	6.4	4.9	15.9	9.1
493.3	200	4.9	8.6	10.5	10.5
505.7	205	6.3	8.5	10.1	12.6
518.0	210	4.2	10.0	15.4	10.9
530.3	215	6.5	11.0	10.4	10.0
542.7	220	6.9	5.7	10.8	13.3
555.0	225	3.8	2.5	5.6	15.6
567.3	230	4.0	3.7	3.4	14.5
579.7	235	5.4	5.1	8.3	16.0
592.0	240	5.0	12.6	18.2	10.7
604.3	245	8.9	14.8	11.8	10.1
616.7	250	8.1	10.8	19.5	9.3
629.0	255	8.0	11.3	24.0	6.8
641.3	260	10.1	11.5	19.8	11.0
653.6	265	7.2	11.3	23.4	6.6
666.0	270	9.5	10.5	16.1	10.5
678.3	275	9.4	5.6	18.3	10.0
690.6	280	9.9	6.6	18.9	9.9
703.0	285	11.4	6.6	23.4	5.1
715.3	290	13.0	8.1	18.3	7.8
727.6	295	9.1	7.3	14.3	13.4

Appendix III. Faunal abundance for 5 common planktic foraminifers (continued)

Cal Yr BP	Core Depth (mm)	<i>G. sacculifer</i> (%)	<i>G. ruber</i> pk (%)	<i>G. ruber</i> wht (%)	<i>N. dutertrei</i> (%)
740.0	300	8.6	8.3	28.6	7.7
752.3	305	6.8	6.2	29.2	10.7
764.6	310	9.9	7.1	20.5	8.1
777.0	315	7.8	8.8	19.5	9.4
789.3	320	10.1	8.0	18.4	9.8
801.6	325	8.4	10.7	23.7	6.8
814.0	330	10.0	12.5	25.7	7.1
826.3	335	6.4	13.5	26.6	6.7
838.6	340	7.2	15.7	23.9	4.6
851.0	345	5.6	14.1	27.0	5.3
863.3	350	8.2	13.1	28.7	7.3
875.6	355	8.1	11.1	21.8	6.8
888.0	360	11.0	7.1	21.2	5.5
900.3	365	8.3	6.3	20.1	8.6
912.6	370	10.0	7.9	29.0	5.9
925.0	375	6.0	5.7	23.5	6.7
937.3	380	5.1	6.8	27.7	5.8
949.6	385	6.4	4.0	19.2	7.6
962.0	390	7.3	4.0	16.2	8.6
974.3	395	8.8	4.4	22.8	6.1
986.6	400	7.5	6.0	18.6	6.9
999.0	405	14.9	3.4	9.0	8.7
1011.3	410	9.9	1.9	11.8	8.9
1023.6	415	7.4	3.2	10.4	11.3
1036.0	420	9.1	4.7	10.3	11.3
1048.3	425	9.5	1.6	10.1	12.3
1060.6	430	10.0	2.2	8.7	8.7
1073.0	435	10.8	7.5	23.3	8.5
1085.3	440	11.9	8.1	26.1	5.4
1097.6	445	7.4	9.3	26.9	8.0

Appendix III. Faunal abundance for 5 common planktic foraminifers (continued)

Cal Yr BP	Core Depth (mm)	<i>G. sacculifer</i> (%)	<i>G. ruber</i> pk (%)	<i>G. ruber</i> wht (%)	<i>N. dutertrei</i> (%)
1110.0	450	10.9	10.0	26.1	3.0
1122.3	455	6.8	6.4	27.0	4.4
1134.6	460	8.6	4.8	17.5	8.3
1147.0	465	10.8	3.7	14.8	4.6
1159.3	470	10.2	4.4	18.7	6.8
1171.6	475	6.6	5.1	18.7	6.3
1184.0	480	9.8	5.7	17.4	5.4
1196.3	485	11.7	6.2	17.9	7.6
1208.6	490	8.8	4.9	26.5	3.9
1221.0	495	6.3	6.3	22.3	4.4
1233.3	500	8.8	10.8	17.8	4.0
1245.6	505	6.3	9.2	23.9	4.6
1258.0	510	11.1	13.9	23.7	5.0
1270.3	515	8.5	8.1	25.9	7.0
1282.6	520	6.4	8.8	25.8	6.8
1295.0	525	7.6	11.7	25.9	6.0
1307.3	530	11.2	9.0	21.3	8.7
1319.6	535	7.6	10.0	26.6	10.0
1332.0	540	10.2	12.2	23.8	6.8
1344.3	545	7.6	12.7	24.1	6.0
1356.6	550	7.0	12.7	27.9	7.0
1369.0	555	3.3	9.6	24.4	6.3
1381.3	560	5.3	10.4	18.2	4.1
1393.6	565	4.9	16.0	18.7	5.8
1406.0	570	10.5	11.5	22.0	4.9
1418.3	575	8.7	10.7	27.7	6.3
1430.6	580	7.1	11.0	20.8	4.5
1443.0	585	7.3	10.0	25.7	5.3
1455.3	590	8.4	8.2	28.0	4.6

Appendix IV. Sea-surface salinity estimates

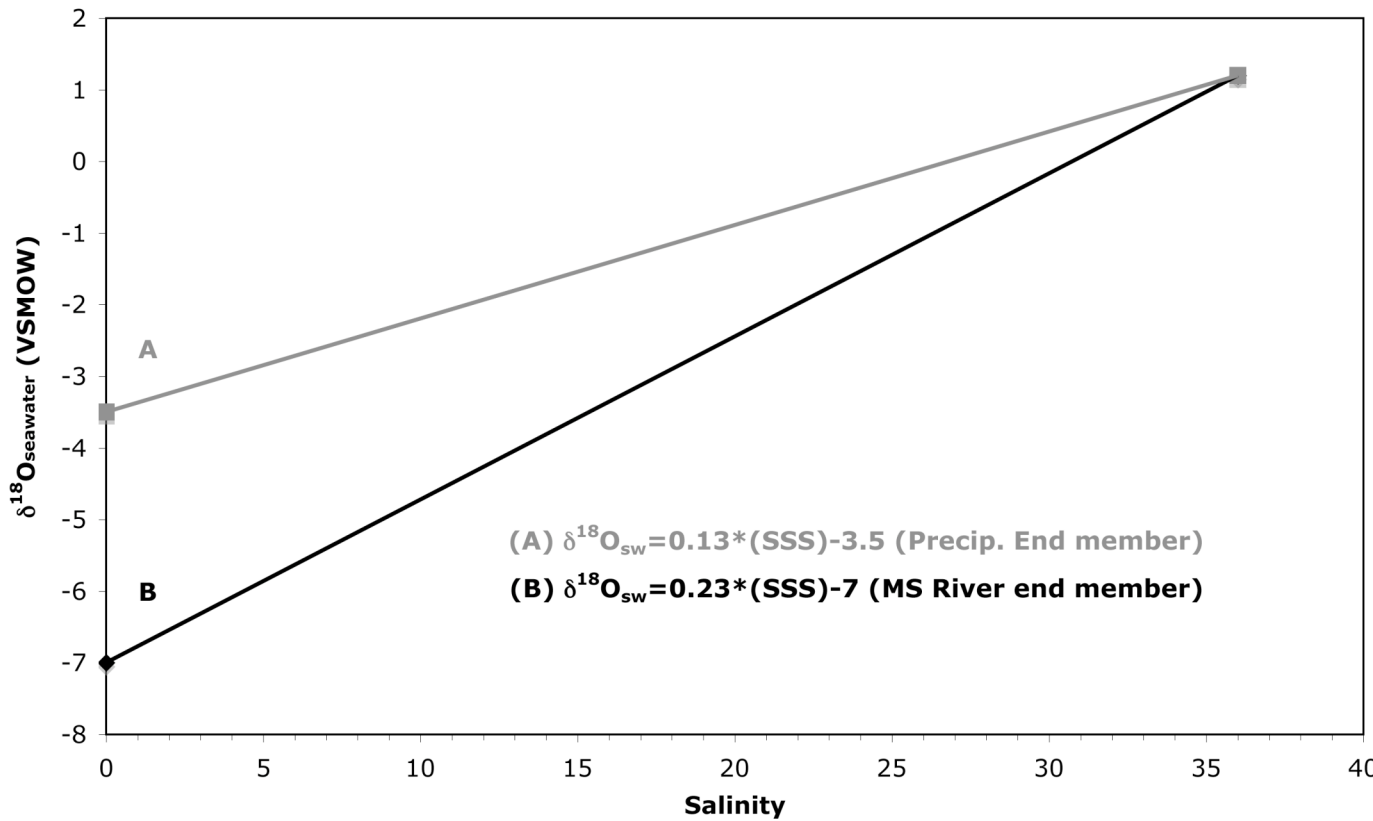


Figure IV.1. Mixing model for estimating sea-surface salinity (SSS) using the modern relationship between $\delta^{18}\text{O}_{\text{seawater}}$ and salinity in the GOM. Precipitation and the Mississippi River (MR) are the 2 sources of freshwater (salinity= 0 psu) to the GOM with modern respective $\delta^{18}\text{O}$ end-members of -3.5‰ (Bowen and Revenaugh, 2004) and -7‰ (Ortner et al., 1995). They are compared with the modern GOM $\delta^{18}\text{O}_{\text{seawater}}$ of 1.2‰ and a salinity of 36 psu (Fairbanks et al., 1992). Note that the slope of the line using a precipitation end-member (A) is much smaller than the slope with the MR end-member (B), and therefore requires larger changes in SSS per unit change in $\delta^{18}\text{O}_{\text{seawater}}$.

Appendix IV. Sea-surface salinity estimates (continued)

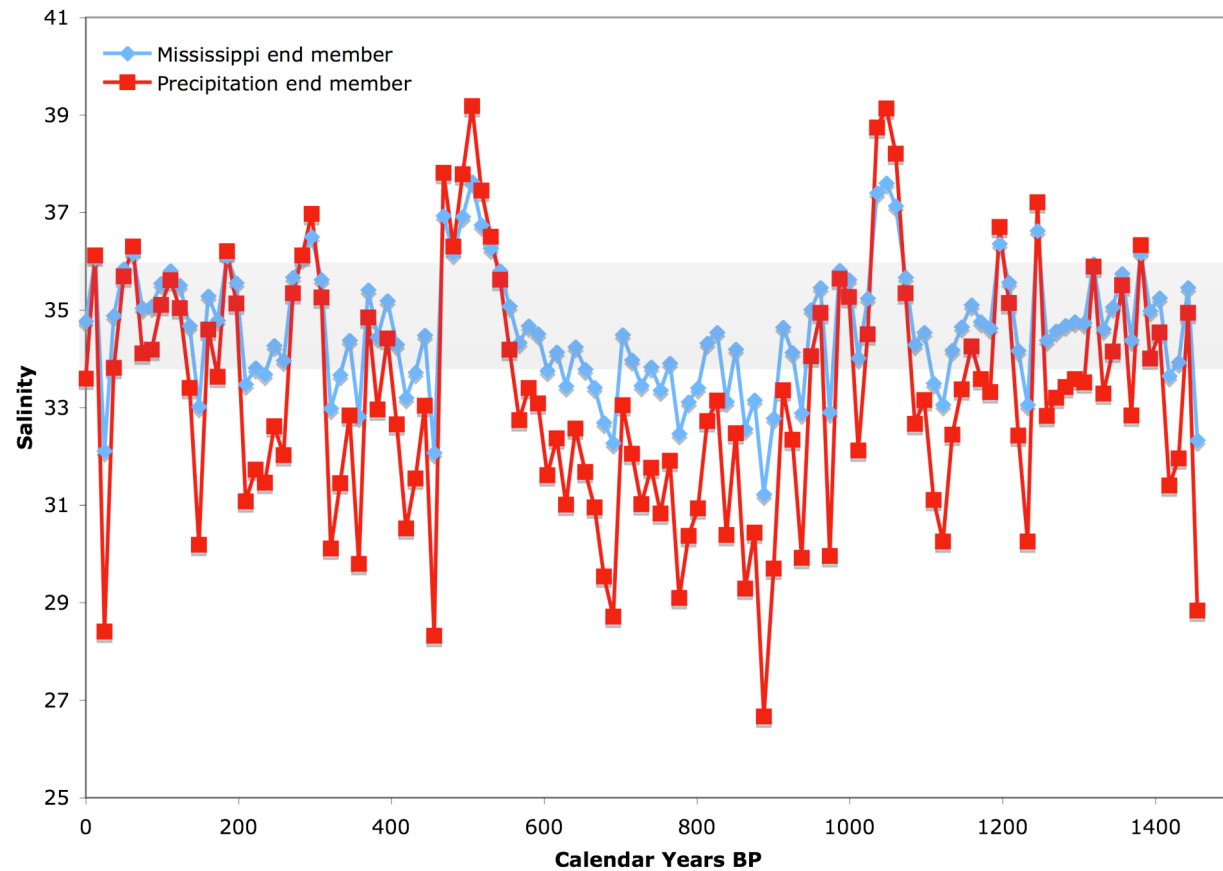


Figure IV.2. Estimated salinity record calculated from Pigmy Basin $\delta^{18}\text{O}_{\text{seawater}}$ using the precipitation $\delta^{18}\text{O}$ end-member of $-3.5\text{\textperthousand}$ (red) and the MR end-member of $-7\text{\textperthousand}$ (blue). The shaded bar represents the modern annual salinity range of 34-36 psu for the GOM (Levitus, 2003). Note that using the precipitation end-member results in an estimated SSS record with a salinity range of 27-39 psu over the past 1400 years. The MR end-member yields a much more reasonable SSS range (32-38 psu).